Spherical to prolate axially symmetric shape transition, $U_{\pi\nu}(5) \rightarrow SU_{\pi\nu}(3)$, in the interacting boson model IBA-2

A. Giannatiempo,[1,2,*] L. Fortunato,[3,4] and A. Vitturi[3,4]

[1]*Dipartimento di Fisica e Astronomia, Università di Firenze, IT-50019 Sesto Fiorentino, Firenze, Italy*

[2]*Istituto Nazionale di Fisica Nucleare, Sezione di Firenze, IT-50019 Sesto Fiorentino, Firenze, Italy*

[3]*Dipartimento di Fisica, Università di Padova, IT-35131 Padova, Italy*

[4]*Istituto Nazionale di Fisica Nucleare, Sezione di Padova, IT-35131 Padova, Italy*

(Received 11 May 2012; published 7 September 2012)

The spherical to prolate deformed shape transition is studied in the framework of the interacting boson IBA-2 model by using a one-parameter Hamiltonian. Excitation energies and $B(E2)$ reduced transition strengths of the ground-state, quasi-β, and quasi-γ bands are considered. Particular attention is payed to effects related to the finite boson number. Structural changes are investigated taking also into account the wave functions of the relevant states. The IBA-2 and X(5) predictions are compared to the experimental data on ^{150}Nd, considered one of the best examples of an X(5)-like nucleus. The analysis of potential energy surfaces of $^{144-156}$Nd, carried out in the framework of the IBA-2 model, provides further information on the structure of the Nd chain and the identification of the phase transition critical point.

DOI: 10.1103/PhysRevC.86.034311 PACS number(s): 21.60.Fw, 21.10.Re, 27.60.+j, 27.70.+q

I. INTRODUCTION

The quantum shape-phase transition as well as the structural evolution of low-lying states of nuclei can be investigated, as a function of proton and/or neutron number, within the framework of the interacting boson approximation (IBA) model [1]. This kind of analysis has usually been carried out in the IBA-1 version of the model, in which no distinction is made between proton pairs and neutron pairs. The nuclear shapes among which the transitions take place are associated with the U(5), O(6), and SU(3) dynamic symmetries of the IBA-1 model, which correspond to a spherical, a γ-unstable, and an axially deformed shape, respectively. Studies performed using the coherent-state formalism [2] in the classical limit (number of nucleons $\rightarrow \infty$) showed that the transitions from U(5) to SU(3) and from U(5) to O(6) are first- and second-order phase transitions, respectively [3].

The phase structure of a two-fluid bosonic system has been investigated [4–8] in the framework of the IBA-2 version of the model [3,9,10], where proton pairs and neutron pairs are treated as distinct constituents. In addition to the three $U_{\pi\nu}(5)$, $O_{\pi\nu}(6)$, and $SU_{\pi\nu}(3)$ symmetries, which correspond to those of the IBA-1 version, a fourth symmetry exists, indicated with $SU^*_{\pi\nu}(3)$, where proton and neutron fluids have different deformations.

A detailed study of the evolution of nuclear structure in a transitional region requires a numerical solution of the Hamiltonian. An analytic (though based on physical approximations) solution for a macroscopic system has been obtained for the critical point (i) of a first-order quantum phase transition from a spherical vibrator to a symmetric deformed rotor, X(5) [11] and (ii) of a second-order quantum phase transition from a spherical vibrator to a γ unstable nucleus, E(5) [12]. These solutions of the Bohr Hamiltonian [13] provide parameter-free (apart from a scale factor) predictions for the excitation energy pattern as well as for the electric quadrupole $B(E2)$ strengths within and among the ground and β bands. The γ bands can also be described with an additional parameter in the X(5) model or in the version introduced by Bijker *et al.* [14], where the separation of variables occurs in a different manner that introduces the dependence on K in the equation for β.

Many studies concerning the properties of the ground state (g.s.) band have been performed with the aim of identifying X(5) candidates [15–28]. In several cases it has been found that nuclei having excitation energies (normalized to that of the 2^+_1 state) very close to the X(5) predictions, have $B(E2)$ reduced transition probabilities [normalized to the $B(E2; 2^+_1 \rightarrow 0^+_1)$] close to the SU(3) limit.

In the present work the transition from a spherical vibrator to an axially symmetric rotor is studied in the framework of the IBA-2 model by using a one-parameter Hamiltonian. The evolution of excitation energies and $B(E2)$ reduced transition strengths of the g.s., quasi-β, and quasi-γ bands are investigated, focusing on effects induced by a finite number of valence nucleons. The analysis of the wave functions of the relevant states, in terms of n_d components, provides significant information on the structure changes of these bands along the whole transition. The IBA-2 results are compared with the IBA-1 ones and to the X(5) predictions. A test of the results is performed by referring to the chain of even neodymium isotopes ($Z = 60$, $N > 82$), which includes ^{150}Nd, one of the first identified X(5)-like nuclei [15,16]. The Hamiltonian parameter has been extracted for each isotope from those obtained in Ref. [29] in the study of the spectroscopic properties of Nd chain. Additional information on the structure of the even $^{144-156}$Nd isotopes is obtained via the IBA-2 study of potential energy surfaces (PESs) performed in the intrinsic state formalism [30–32], using the parameters of Ref. [29].

In Sec. II, the spherical-to-prolate deformed shape transition is investigated in the framework of the IBA-2 model and

*giannatiempo@fi.infn.it

the results are compared with the IBA-1 ones and with the X(5) predictions. A test of the findings of Sec. II, performed by referring to the experimental data concerning heavy Nd isotopes and $N = 90$ even isotones, is discussed in Sec. III. The PES calculations are reported in Sec. IV. Finally, the main conclusions of this study are drawn in Sec. V.

II. SPHERICAL-TO-PROLATE AXIALLY DEFORMED SHAPE TRANSITIONS IN IBA AND X(5) MODELS

The X(5) analytic solution of the Bohr Hamiltonian for the critical point of the phase transition from a spherical vibrator to a prolate symmetric rotor was obtained by Iachello [11] by separating the potential into two terms. The quadrupole deformation parameter, β, has been associated with an infinite square-well potential, and the triaxiality deformation parameter, γ, with a harmonic oscillator potential. In this model the $n_\gamma = 0$ bands built on the $0_1^+, 0_2^+$, and 0_3^+ states are classified as $s = 1$, $s = 2$, and $s = 3$ bands, respectively. The predictions for excitation energies and $E2$ transition probabilities are parameter free (except for scale). An additional parameter in the γ-dependent part makes it possible to model also γ-vibrational bands [11]. Alternatively, one can use the approach of Bijker *et al.* [14] in the limit of small oscillations in the γ variable.

In the IBA-1 model the U(5)-to-SU(3) transition can be described by a schematic Hamiltonian (see, e.g., Ref. [33]) governed by just one control parameter, ζ, namely,

$$H(\zeta) = c\left[(1-\zeta)\hat{n}_d + \frac{\zeta}{4N_B}\hat{Q}^{(\chi)}\cdot\hat{Q}^{(\chi)}\right], \qquad (1)$$

with χ fixed at the value $-\sqrt{7}/2$. Here, c is a normalization factor, $\hat{n}_d$ is the d-boson number operator, and N_B is the total boson number. The expression of the quadrupole operator is given by

$$\hat{Q} = [d^\dagger \times \tilde{s} + s^\dagger \times \tilde{d}]^{(2)} + \chi[d^\dagger \times \tilde{d}]^{(2)}. \qquad (2)$$

In the calculations performed in the present work the value of χ in the $E2$ transition operator

$$\hat{T}(E2) = e\hat{Q}^{(\chi)} \qquad (3)$$

is the same as in the Hamiltonian (consistent-Q formalism [34,35]); e is the effective quadrupole charge.

The studies by McCutchan *et al.* [33] and Rosensteel and Rowe [36], both performed using Hamiltonian (1), are of particular relevance to our findings. In Ref. [33] the differences between the predictions of the X(5) model and the IBA-1 calculations, concerning the excitation energies of the g.s. band in the phase transition region, have been pointed out. The ζ parameter has been allowed to vary from 0 to 1 and χ from 0 to $-\sqrt{7}/2$ so as to investigate the whole Casten's triangle [37]. It has been found that no set of IBA-1 parameters can exactly reproduce the X(5) solution. Rosensteel and Rowe [36] studied thoroughly the dependence of the U(5)-to-SU(3) phase transition on the the finite boson numbers. Their conclusions support the idea that a close correspondence between a first-order phase transition in a macroscopic system and a transition in a corresponding system with a discrete number of nucleons exists only for a large number of particles.

As for the IBA-2 model, the physically dominant interactions contained in the Hamiltonian

$$H = \varepsilon_\pi \hat{n}_{d_\pi} + \varepsilon_\nu \hat{n}_{d_\nu} + \kappa_{\pi,\pi}\,\hat{Q}_\pi^{(\chi_\pi)}\cdot\hat{Q}_\pi^{(\chi_\pi)} + \kappa_{\nu,\nu}\,\hat{Q}_\nu^{(\chi_\nu)}\cdot\hat{Q}_\nu^{(\chi_\nu)} + \kappa_{\pi\nu}\,\hat{Q}_\pi^{(\chi_\pi)}\cdot\hat{Q}_\nu^{(\chi_\nu)} + \hat{M}_{\pi\nu}(\xi_i) \qquad (4)$$

[d-boson number $\hat{n}_{d_\rho}$, $(\rho = \pi, \nu)$, quadrupole-quadrupole, and Majorana operators] give rise to four dynamical symmetries. The three of them that occur for $\chi_\pi = \chi_\nu$ correspond to the U(5), O(6), and SU(3) symmetries of the IBA-1 model. In the IBA-2 model the $U_{\pi\nu}(5)$ dynamical symmetry is realized when $\kappa_{\pi,\pi} = \kappa_{\nu,\nu} = \kappa_{\pi\nu} = 0$ and the $SU_{\pi\nu}(3)$ dynamical symmetry when $\varepsilon_\pi = \varepsilon_\nu = 0$ and $\chi_\pi = \chi_\nu = -\sqrt{7}/2$. The Majorana operator affects only the excitation energies of mixed-symmetry (MS) states.

The $E2$ transition operator is given by

$$\hat{T}(E2) \equiv e_\nu\hat{T}_\nu(E2) + e_\pi\hat{T}_\pi(E2) = e_\nu\hat{Q}_\nu + e_\pi\hat{Q}_\pi, \qquad (5)$$

where the parameters e_π and e_ν are the quadrupole effective charges.

To investigate the $U_{\pi\nu}(5)$-to-$SU_{\pi\nu}(3)$ transition we adopted the one-parameter Hamiltonian

$$H = c\left[(1-\zeta)(\hat{n}_{d_\pi} + \hat{n}_{d_\nu}) + \frac{\zeta}{4N_B}\left(\hat{Q}_\pi^{(\chi_\pi)}\cdot\hat{Q}_\nu^{(\chi_\nu)}\right)\right]. \qquad (6)$$

This expression is similar to that of Hamiltonian (1). The boson number is the sum of the proton bosons N_π and neutron bosons N_ν. The first term gives the $U_{\pi\nu}(5)$ dynamical symmetry; the second one, with χ_π and χ_ν kept fixed to $-\sqrt{7}/2$, can be connected to the $SU_{\pi\nu}(3)$ dynamical symmetry. In fact the operator $(\hat{Q}_\pi^{(\chi_\pi)}\cdot\hat{Q}_\nu^{(\chi_\nu)})$, if $\chi_\pi = \chi_\nu = -\sqrt{7}/2$, can be written as a combination of the Casimir operators of the algebras appearing in the $SU_{\pi\nu}(3)$ dynamical symmetry (cf. Eq. (2.4) in Ref. [7]), namely,

$$2\left(\hat{Q}_\pi^{(\chi_\pi)}\cdot\hat{Q}_\nu^{(\chi_\nu)}\right) = C(SU_{\pi\nu}(3)) - C(SU_\pi(3)) - C(SU_\nu(3)). \qquad (7)$$

Hereafter, the $(\hat{Q}_\pi^{(\chi_\pi)}\cdot\hat{Q}_\nu^{(\chi_\nu)})$ term $(\chi_\pi = \chi_\nu = -\sqrt{7}/2)$ is referred to as the $[SU_{\pi\nu}(3)]$ Hamiltonian. The brackets indicate that the quadrupole interactions between like-nucleons are neglected. This choice is justified by the dominant role played by the proton-neutron quadrupole interaction in producing collective nuclear deformation (see, e.g., [38]). In the analysis, the Majorana parameters are kept fixed at 2 MeV. States of MS origin, which do not have counterparts in the IBA-1 states, are pushed to such high energies that only fully symmetric (FS) states are present in the energy region of interest. This allows the comparison of the IBA-2 results with the IBA-1 ones and, as far as the critical point of the transition is concerned, with the X(5) predictions. Because the Majorana term does not affect the results reported in this section it does not appear explicitly in Eq. (6). In the calculations, carried out using the NPBOS code [39], the value of χ_ρ in Eq. (5) was fixed at $-\sqrt{7}/2$.

Many of the examples presented in the following subsections refer to a nucleus having $N_\pi = 5$. This is helpful for the comparison of the IBA-2 and X(5) predictions with the experimental data concerning the neodymium chain, presented in Sec. III.

A. Ground-state band

The phase transitional behavior is commonly described in terms of some observable that characterizes the degree of deformation of a nucleus. The $(E4_1^+)/E(2_1^+)$ ratio $[R_{4/2}]$ is usually adopted as a simple benchmark. As remarked in Ref. [36], only for sufficiently large N_B the transition happens in a narrow region around the critical value of the control parameter ζ. An example of the dependence of the transition width on the number of the valence bosons is shown in Fig. 1. The $R_{4/2}$ values calculated with Hamiltonian (1) and Hamiltonian (6) are reported in the upper panel, as a function of ζ, for different N_B values. The values predicted by the X(5) model and by the $\mathrm{U(5)} = \mathrm{U}_{\pi\nu}(5)$ and $\mathrm{SU(3)} = [\mathrm{SU}_{\pi\nu}(3)]$ limits are also shown. The width of the critical zone decreases with N_B, however, a sufficiently sharp behavior at the critical point is not yet achieved for $N_B = 12$. Because of the normalization adopted in Hamiltonian (6) the IBA-2 curves do not cross exactly at the same value of ζ. This would be the case if the terms $\hat{n}_{d_\rho}$, $\hat{Q}_\rho$ were divided by N_ρ in the adopted Hamiltonian. However, Hamiltonian (6) is preferable for relating the present calculations to those performed in Ref. [29] for the Nd chain (see Sec. III).

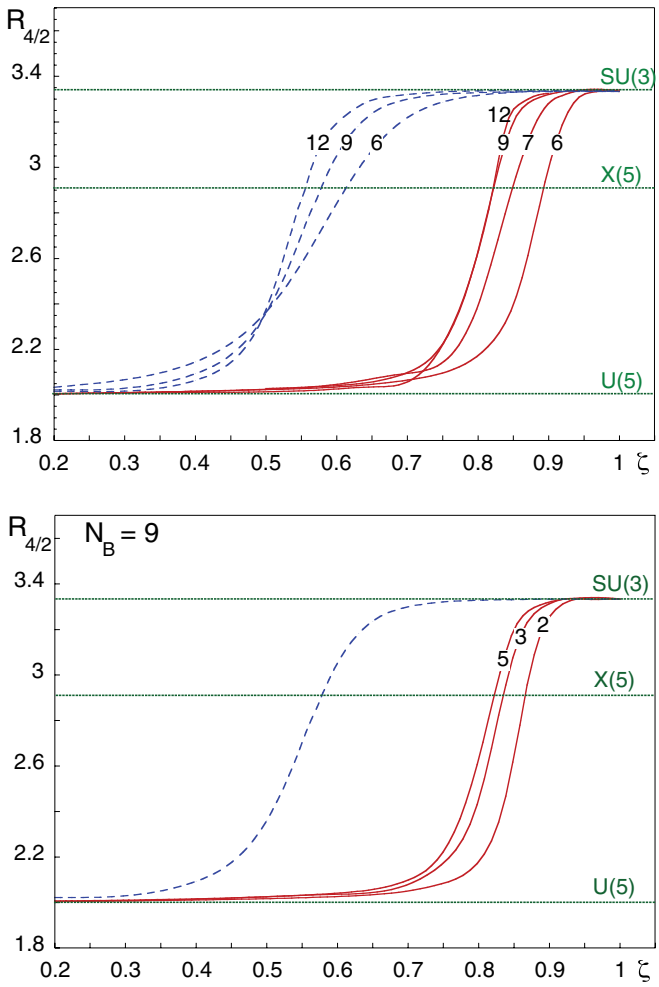

FIG. 1. (Color online) Normalized excitation energies of the 4_1^+ state in the IBA-1 (dashed lines) and IBA-2 (solid lines) versions of the model, as a function of ζ, for (upper panel) different values of N_B, reported on each curve (IBA-2 values correspond to $N_\pi = 5$) and (bottom panel) $N_B = 9$, with the different N_π boson numbers reported on each IBA-2 curve. Values predicted by the U(5) and SU(3) limits and by the X(5) model are indicated by horizontal lines.

The $R_{4/2}$ ratios calculated for a given boson number $(N_B = 9)$, with Hamiltonian (1) and Hamiltonian (6) (varying N_π) are reported in the lower panel in Fig. 1. In the IBA-2 calculations the symmetry breaking induced by the lack of the quadrupole interactions between like nucleons gives rise to a splitting of the curves corresponding to different values of N_π and N_ν. This depends on the relative strength of the π-ν interaction that induces deformation (related to the value of the $N_\pi N_\nu$ product) and the pairing interaction (related to the value of $N_\pi + N_\nu$). Indeed, in the example shown in the figure, the $N_\pi = 5$ curve achieves first the X(5) critical $R_{4/2}$ value.

The normalized excitation energies, $R[E]$, of the g.s. band take the same values for *corresponding* values of ζ in Hamiltonians (1) and (6), e.g., for ζ values which lead to the same $R_{4/2}$ value.

The $R[E]$ values of the g.s. band predicted by the X(5) model are given, as a function of J, in the left panel in Fig. 2. They are compared to the values calculated in the IBA-1 model for $N_B = 6$ and in the IBA-2 model for $N_B = 12$ $(N_\pi = 5)$, in both cases keeping the parameter ζ to the value for which $R_{4/2}$ takes the value 2.91 predicted by the X(5) model. Hereafter, this value is referred to as $\zeta[\mathrm{X(5)}]$. The two IBA curves, which exactly overlap, are close to that representing the X(5) predictions only for small J, lying slightly higher for high J (this extends to the IBA-2 case the findings of Ref. [33] already mentioned). For $\zeta[\mathrm{X(5)}]$ the deformation predicted by the IBA model for the g.s. band is therefore slightly higher than that predicted by the X(5) solution. In the transition region very small changes of ζ give rise to strong variations of the curve slopes. This is shown in the right panel in Fig. 2, where the $R[E]$ values of the g.s. band are reported, as a function of J, with ζ as order parameter, for an $N_\pi = 5$, $N_\nu = 4$ nucleus. By reducing ζ by about 2% with respect to $\zeta[\mathrm{X(5)}] = 0.82$ (see bottom panel in Fig. 1), the relevant curve falls below the X(5) curve.

The values of the normalized $B(E2)$ strengths, $R[B(E2)]$, of the g.s. band, calculated in the IBA-2 model, are equal to (only slightly different from) the IBA-1 values, despite the presence of two effective charges in Eq. (5). The IBA-1 values are always independent of the effective charge, because of the expression of the $E2$ transition operator. In the $\mathrm{U}_{\pi\nu}(5)$ limit the ratio $\langle J_f \parallel \hat{T}(E2)_\pi \parallel J_i\rangle / \langle J_f \parallel \hat{T}(E2)_\nu \parallel J_i\rangle$ equals N_π/N_ν and in the $[\mathrm{SU}_{\pi\nu}(3)]$ limit $\langle J_f \parallel \hat{T}(E2)_\nu \parallel J_i\rangle$ is equal to $\langle J_f \parallel \hat{T}(E2)_\pi \parallel J_i\rangle$ for $N_\pi = N_\nu$. In both cases the normalized $B(E2)$ values are independent of the values of the effective charges and are the same as in the U(5) and SU(3) limit, respectively. In the $[\mathrm{SU}_{\pi\nu}(3)]$ limit there are, instead, some differences between the IBA-1 and the IBA-2 values when $N_\pi \neq N_\nu$, as shown in the left panel in Fig. 3. Here, the IBA-2 values are reported, as a function of J, for different values of N_B and of e_π and e_ν, together with the corresponding IBA-1 ones. The spread of the IBA-2 values around the IBA-1

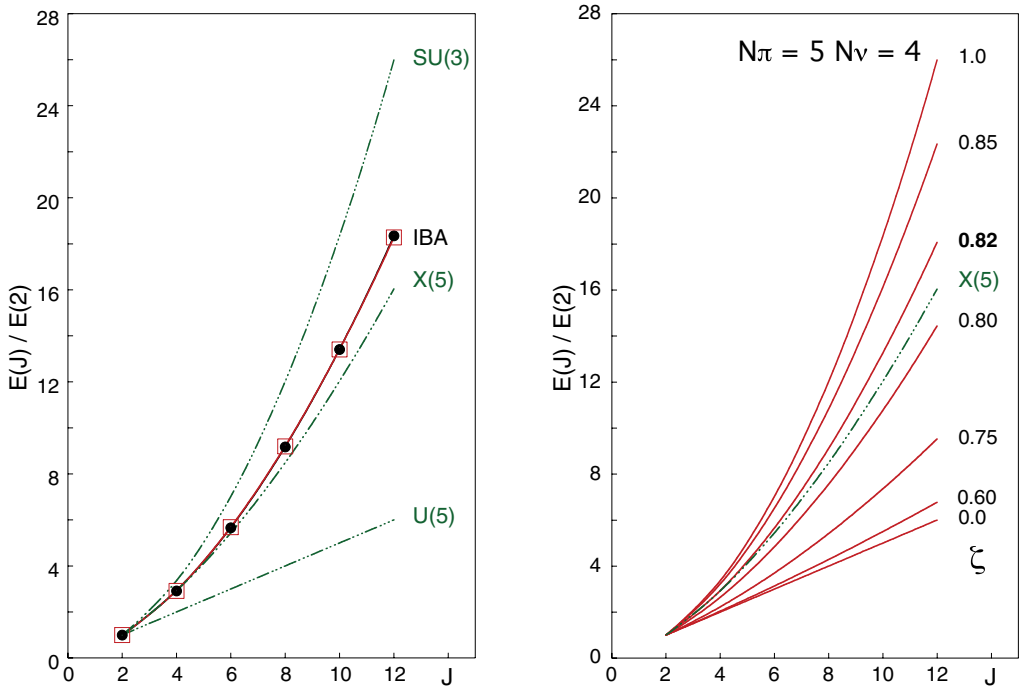

FIG. 2. (Color online) Normalized excitation energies of the g.s. band, as a function of J. Left: IBA-1 (filled circles) values for $N_B = 6$ and IBA-2 (open squares) values for $N_B = 12$ ($N_\pi = 5$, $N_\nu = 7$), calculated for $\zeta = \zeta$[X(5)], are shown together with the U(5), SU(3), and X(5) predictions. Right: IBA-2 values of a nucleus having $N_\pi = 5$ and $N_\nu = 4$ calculated for the ζ values reported close to each curve. The ζ[X(5)] value is in boldface.

value is limited to a few percent also in the case of $N_\pi = 5$ and $N_\nu = 1$, where the difference between the number of π and that of ν bosons is the largest among the considered cases. Therefore, the normalized $E2$ strengths of the g.s. band are independent, or nearly independent, of the effective charges also in the the IBA-2 model.

The behavior of the $R[B(E2)]$ strengths, reported in the center panel in Fig. 3, as a function of J, can be compared with that of the $R[E]$ values, shown in Fig. 2 for the same nucleus ($N_\pi = 5$, $N_\nu = 4$) and for the same values of the order parameter ζ. The X(5) curve, which, in Fig. 2, is in a region limited by the $\zeta = 0.80$ and 0.82 curves, is no longer confined in a narrow band of ζ values. Besides, the $R[B(E2)]$ curves calculated for $\zeta \simeq 0.82$ do not fall in a region midway between the $U_{\pi\nu}(5)$ ($\zeta = 0$) and the $[SU_{\pi\nu}(3)]$ ($\zeta = 1$) limits. They are close to the X(5) curve only up to $J = 4$ and get close to the $[SU_{\pi\nu}(3)]$ limit for higher J.

The $R[B(E2)]$ strengths of the $4_1^+ \to 2_1^+$ and $6_1^+ \to 4_1^+$ transitions, for an $N_\pi = 5$, $N_\nu = 4$ nucleus, are shown, as a function of ζ, in the right panel in Fig. 3. Their values start rising with respect to the $U_{\pi\nu}(5)$ value for $\zeta \approx 0.4$ and, after

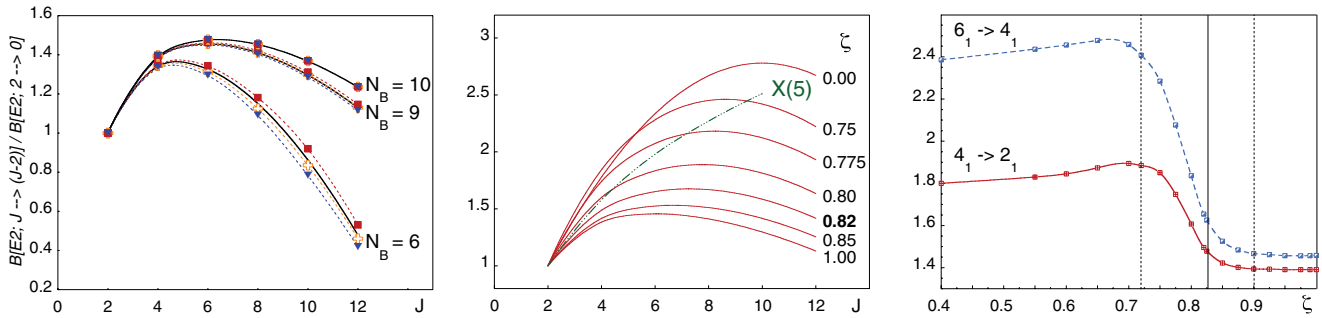

FIG. 3. (Color online) Left: Normalized $B(E2)$ transition strengths of the g.s. band, as a function of J, for different N_B in the SU(3) limit (solid lines) and in the IBA-2 ($N_\pi = 5$) (dashed lines) model for $\zeta = 1.0$. For each N_B the IBA-2 values calculated for $e_\pi = e_\nu$ (crosses), $e_\pi = 2e_\nu$ (triangles), and $e_\pi = 0.5e_\nu$ (squares) are shown. Center: Normalized $B(E2)$ values of the g.s. band of a nucleus having $N_\pi = 5$ and $N_\nu = 4$, as a function of J, for the values of the order parameter ζ reported close to each curve. The values predicted by the X(5) model are shown as the dotted-dashed line. Right: IBA-2 normalized $B(E2)$ strengths of the $4_1^+ \to 2_1^+$ and $6_1^+ \to 4_1^+$ transitions, reported as a function of ζ for an $N_\pi = 5$, $N_\nu = 4$ nucleus.

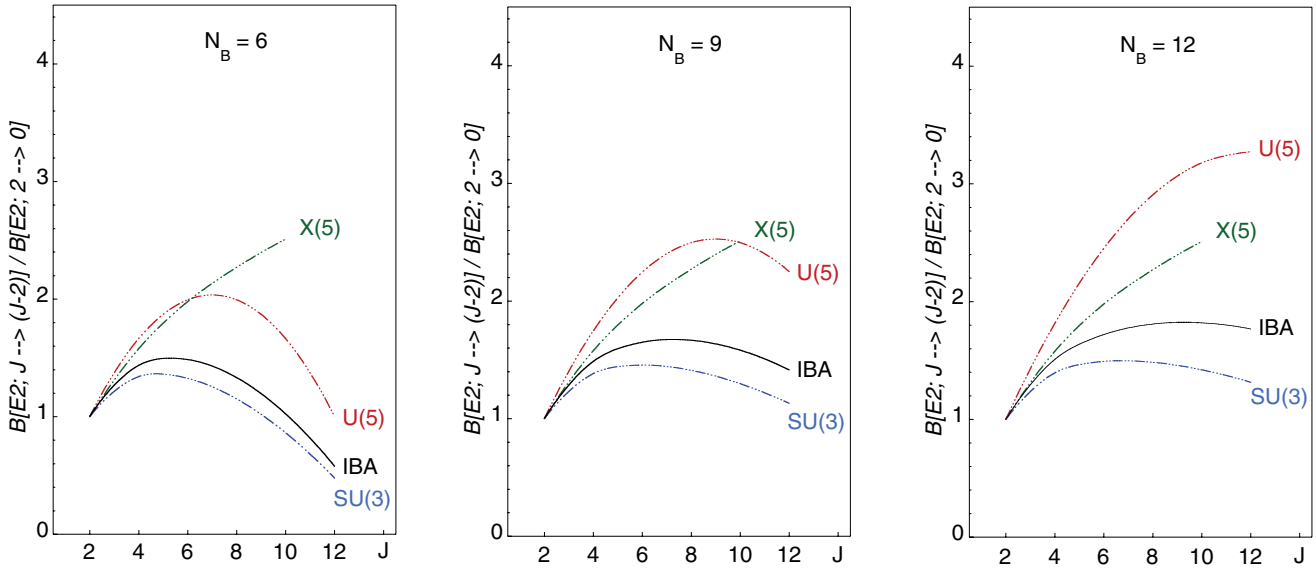

FIG. 4. (Color online) Normalized $B(E2)$ values of the g.s. band, calculated in the framework of the IBA-1 model for ζ[X(5)], compared to the values predicted by the X(5) model and by the U(5) and SU(3) symmetries for the N_B values shown.

having reached a maximum for $\zeta \approx 0.70$, rapidly decrease up to $\zeta \approx 0.90$. In the 0.90–1.0 range of ζ the $R[B(E2)]$ strengths are close to those predicted by the $[\mathrm{SU}_{\pi\nu}(3)]$ limit. In this panel and in the right panel in Fig. 2, one can see how $BE(2)$ and energy ratios, respectively, remain fairly constant around the limits (thus displaying the hallmarks of a quasidynamical symmetry) and that the change happens swiftly only in the region around the critical point.

Because in the IBA model the normalized $B(E2)$ values of the g.s. band strongly depend on the boson number, the $R[B(E2)]$ curves representing the U(5) and SU(3) predictions as well as the IBA values for ζ[X(5)] move with respect to the X(5) curve as N_B changes. Some examples are given in Fig. 4. For $N_B = 12$ the X(5) curve is located between the U(5) and the SU(3) curves. However, as the boson number decreases, the curves representing the two IBA limits move down, the curvatures increase, and a maximum appears in the U(5) curves for a value of J close to N_B. The region included between the two limits narrows, and for small N_B, the normalized $B(E2)$ values predicted by the U(5) limit can diminish sufficiently to become close, for small values of J, to those predicted by the X(5) model. Therefore, the whole X(5) curve is no longer included in the U(5)-SU(3) region. As N_B diminishes, owing to the increasing importance of the finite-number effect on the magnitude of $R[B(E2)]$, the X(5) predictions go more and more off the mark. A close correspondence between X(5) and IBA predictions on $B(E2)$ strengths can therefore be obtained only when the boson number is very large (>12). These findings are in agreement with the conclusions drawn in Ref. [36].

Further information on the structure evolution of the g.s. band in the $\mathrm{U}_{\pi\nu}(5) \rightarrow [\mathrm{SU}_{\pi\nu}(3)]$ transition can be obtained from the wave functions. The percentage of the n_d components for the 0_1^+, 2_1^+, and 4_1^+ states in a nucleus having $N_\pi = 5$ and $N_\nu = 4$ is reported in Fig. 5 for some values of ζ of particular interest. The structure of these states is very close to that of the $\mathrm{U}_{\pi\nu}(5)$ symmetry up to $\zeta \simeq 0.60$, then starts changing. At the beginning of the transition region ($\zeta \approx 0.75$)

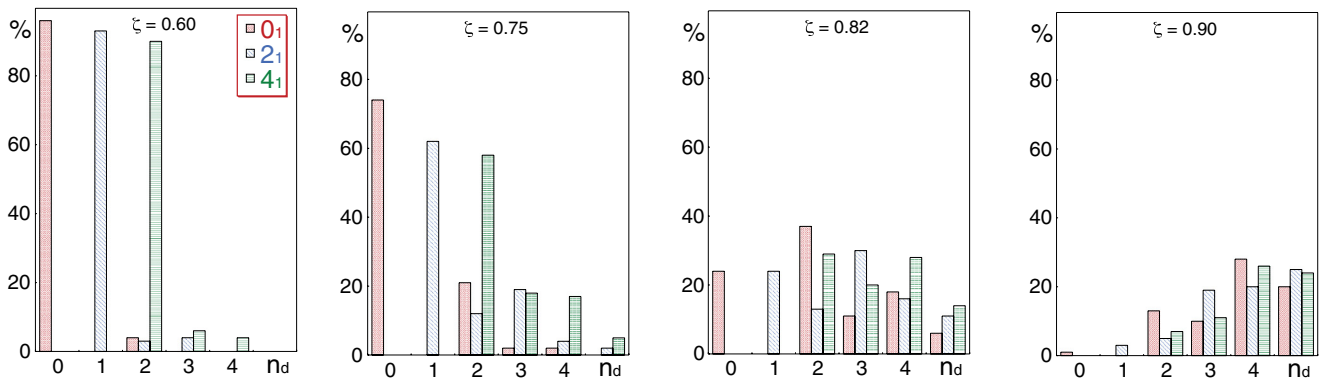

FIG. 5. (Color online) Percentage of the n_d components of the 0_1^+, 2_1^+, and 4_1^+ states in a nucleus having $N_\pi = 5$ and $N_\nu = 4$ for the values of ζ shown in each panel.

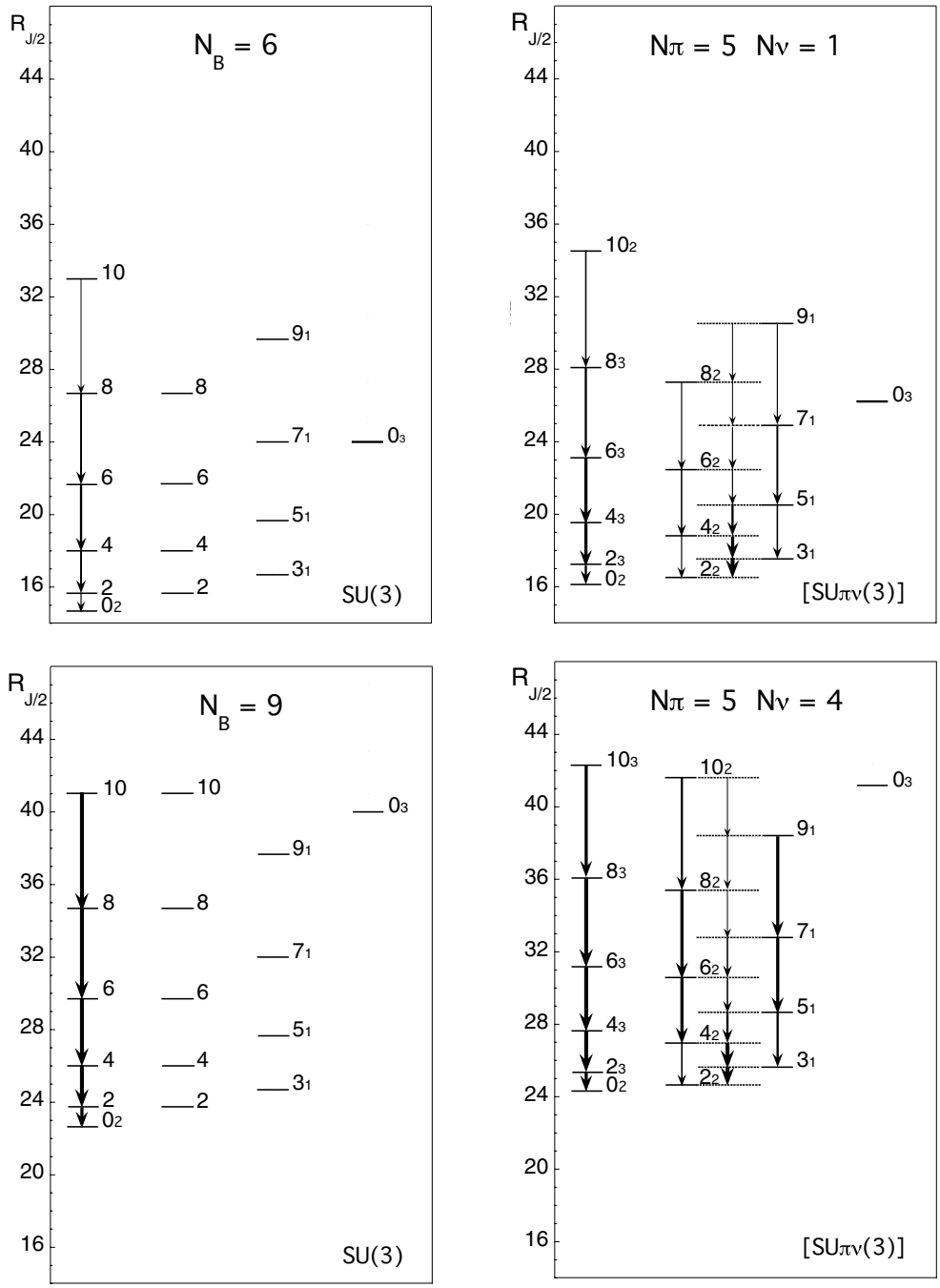

FIG. 6. Level scheme and relative $B(E2)$ strengths of the quasi-β and quasi-γ bands for nuclei having $N_B = 6$ and 9 in the SU(3) and [$SU_{\pi\nu}(3)$] limits. The 0_3^+ level is also shown. The arrow thickness reflects the normalized $E2$ strength of the transition.

the $n_d = 0$, 1, and 2 components are still the predominant ones in the wave functions of the 0_1^+, 2_1^+, and 4_1^+ states, respectively. For $\zeta[\mathrm{X}(5)] = 0.82$ several n_d components of comparable intensities are present. The evolution toward a deformed structure continues without further discontinuities for increasing ζ. For $\zeta = 0.90$ the percentage of the lowest n_d components is strongly reduced. As expected in the deformed limit the wave functions, diagonalized in the spherical basis, have no dominant component and appear to be strongly admixed.

B. Quasi-β and quasi-γ bands

For even-even nuclei the terms quasi-β and quasi-γ bands are normally used for spherical regions, and the corresponding ones, β and γ bands, for deformed regions. For simplicity, we use the term "quasiband" without distinction when describing the whole evolution of these bands.

In the U(5) or $U_{\pi\nu}(5)$ limit, one can refer to the quasi-β band and quasi-γ band as those made up by the $0_2^+[2d]$, $2_3^+[3d]$, $4_3^+[4d]$, $6_3^+[5d]$, ... states and by the $2_2^+[2d]$, $4_2^+[3d]$, $6_2^+[4d]$,

$8_2^+[5d]$, . . . states, respectively. The d-boson quantum number of each state is given in parentheses. Strong $E2$ transitions connect the J, $J-2$, and $\Delta n_d = 1$ states in each band.

The values of both $R[E]$ and $R[B(E2)]$ ratios of quasi-β and quasi-γ bands are equal in the U(5) and $U_{\pi\nu}(5)$ limits. This is not the case in the SU(3) and $[SU_{\pi\nu}(3)]$ limits. In the IBA-1 limit the levels of the β and γ bands of the same J are degenerate, whereas they are not in the IBA-2 limit. As for the normalized $B(E2)$ strengths, the IBA-2 values calculated for $e_\pi = e_\nu$, $e_\pi = 2e_\nu$, and $e_\pi = 0.5e_\nu$ differ from each other by at most a few percent, for both quasi-β and quasi-γ bands, analogously to what happens for the g.s. band (see left panel in Fig. 3). This is also the largest difference with respect to the IBA-1 values of the quasi-β band, the values of which have been calculated analytically [40]. Because also the $R[B(E2)]$ strengths of the quasi-β and quasi-γ bands, like those of the g.s. band, are nearly independent of e_π and e_ν, the whole IBA-2 study is performed by varying practically only the ζ parameter.

The excitation energy and decay patterns of the β and γ bands in the SU(3) and $[SU_{\pi\nu}(3)]$ limits are shown in Fig. 6, together with the excitation energy of the 0_3^+ level, for nuclei having $N_B = 6$ and 9. The normalized energies of the two bands increase rapidly from $N_B = 6$ to $N_B = 9$. In the $[SU_{\pi\nu}(3)]$ limit the J_i memberships of each band are identified on the basis of the $B(E2)$ strengths of the de-exciting transitions. The states of the β band with $J > 0$ have index $i = 3$; the even ones of the γ band index $i = 2$.

The dependence of the normalized excitation energies $E(J)/E(2)$ on N_B, as the deformation increases, is shown for the quasi-β band in Fig. 7, considering again (see Fig. 2, left panel) the cases of $N_B = 6$ and 9. Here, the $R[E]$ values predicted by the X(5) model and by the $U_{\pi\nu}(5) = U(5)$, SU(3), and $[SU_{\pi\nu}(3)]$ limits are reported, as a function of J, together with those calculated for ζ[X(5)] in the IBA-1 and IBA-2 versions of the model. In moving away from the U(5) limit the curves corresponding to the two values of N_B start splitting. In the transition region they are completely separated, whereas the difference between the IBA-1 and the IBA-2 values of the ζ[X(5)] curves corresponding to the same N_B is still very small. At variance with what happens for the g.s. band, the ζ[X(5)] curves lie below the X(5) curve, which they approach for increasing N_B. The separation between the curves of different N_B values and between the IBA-1 and the BA-2 curves with the same N_B becomes remarkable when the deformation attains its maximum value.

Similarly to what happens for the g.s. band, the smaller the boson number, the more the $R[B(E2)]$ strengths of the quasi-β and quasi-γ bands calculated for ζ[X(5)] differ from the X(5) predictions. This is shown in Fig. 8, where the normalized $B(E2)$ values of the $U_{\pi\nu}(5)$ and $[SU_{\pi\nu}(3)]$ limits are reported, as a function of J, for $N_B = 6$ and 9 ($N_\pi = 5$), together with the X(5) predictions and the IBA-2 values calculated for ζ[X(5)]. For clarity, the values of the transitions connecting even-J and odd-J memberships of the quasi-γ band are shown separately. The general features are similar to those of the g.s. band (see Fig. 4). Indeed, for $N_B = 6$ the $U_{\pi\nu}(5)$ curves have a maximum close to (not far from) $J = 6$. In going towards higher N_B ($N_B = 9$ in the present example) the $U_{\pi\nu}(5)$ values increase noticeably and the maximum moves towards

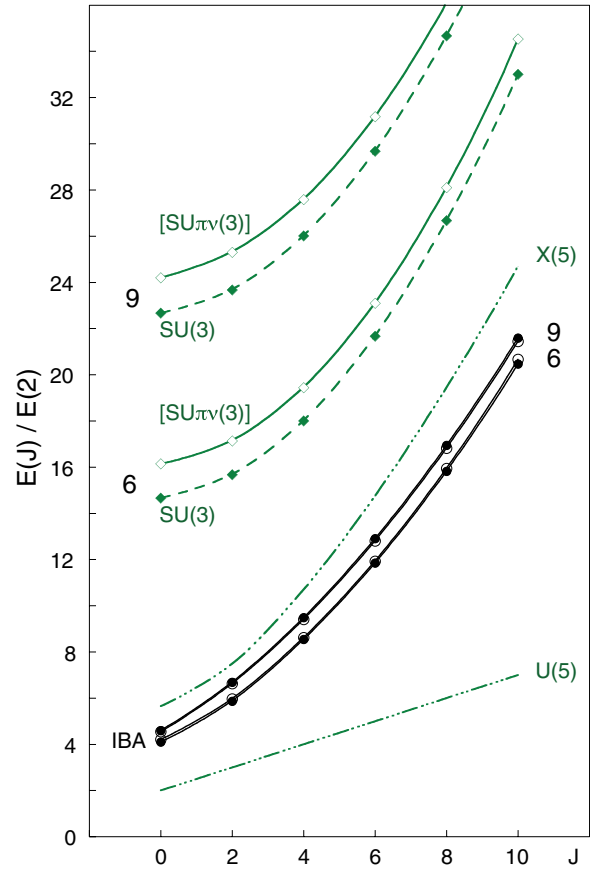

FIG. 7. (Color online) Normalized excitation energies of the quasi-β band, as a function of J, for $N_B = 6$ and 9. The values calculated for ζ[X(5)] in the IBA-1 and IBA-2 ($N_\pi = 5$) models are represented by filled and open symbols, respectively. The values of the U(5), SU(3), and $[SU_{\pi\nu}(3)]$ limits are also shown, together with those of the X(5) model.

higher J or disappears, whereas the $[SU_{\pi\nu}(3)]$ curves, after an initial increase, tend to become quite flat. The X(5) curve, for $N_B = 6$, crosses (left and center panels) or lies higher than (right panel) the $U_{\pi\nu}(5)$ curve, whereas for $N_B = 9$, it is included in the region defined by the $U_{\pi\nu}(5)$ and $[SU_{\pi\nu}(3)]$ curves, except for its highest odd spin. Also, the behavior of the ζ[X(5)] curves is similar to that observed in the g.s. band for $N_B = 6$ and 9. Indeed, in all cases considered, they are quite close to those of the $[SU_{\pi\nu}(3)]$ limit.

A more detailed IBA-2 analysis of the evolution of the quasi-β and quasi-γ bands, as a function of ζ, is presented hereafter for a nucleus having $N_\pi = 5$, $N_\nu = 4$. The normalized excitation energies of the even-J_i states, with $i = 2, 3$ and $J_{\max} = 6$ are reported, as a function of ζ, in Fig. 9, together with the $U_{\pi\nu}(5)$ and $[SU_{\pi\nu}(3)]$ values. The comparison with the X(5) predictions is limited to the excitation energies of the $s = 2$ band to avoid the introduction of the additional normalization required for the quasi-γ band. The 0_3^+ level is also considered, as it provides further information on the nuclear structure evolution.

The degeneracy of the 0_2^+-2_2^+, 0_3^+-2_3^+-4_2^+, and 4_3^+-6_2^+ states, present in the $U_{\pi\nu}(5)$ limit, starts disappearing for $\zeta \simeq 0.60$. No noticeable increase in the $R[E]$ values is, however,

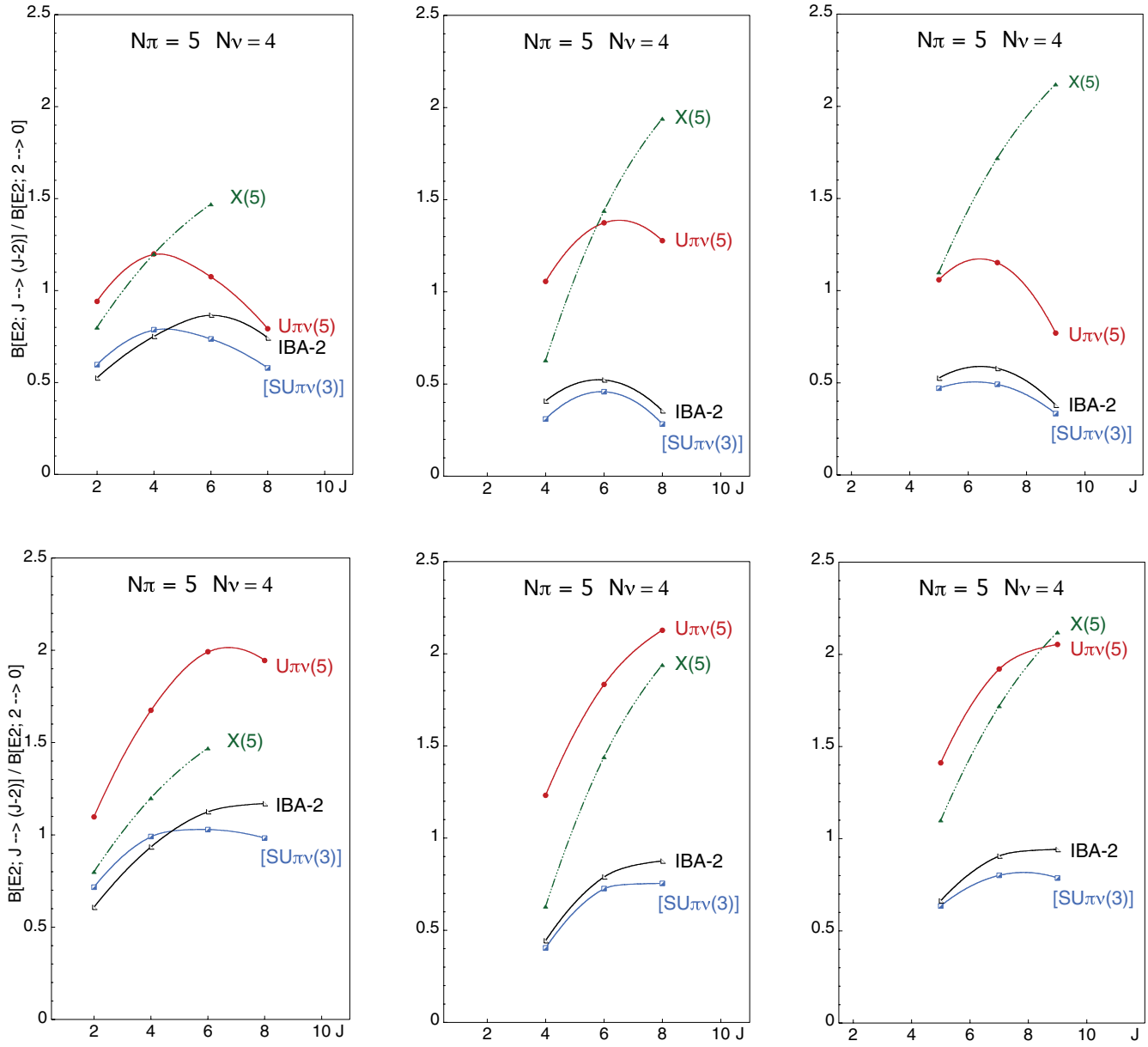

FIG. 8. (Color online) Normalized $B(E2)$ values of the quasi-β-band (left) and of the even-J states (middle) and odd-J states (right) of the quasi-γ band calculated for ζ[X(5)] in the IBA-2 model and predicted by the $U_{\pi\nu}(5)$ and $[SU_{\pi\nu}(3)]$ limits and by the X(5) model. The data for $N_B = 6$ are reported in the upper panels; those for $N_B = 9$, in the lower panels.

observed up to $\zeta \approx 0.72$; thereafter the excitation energies of the states of the quasi-β and quasi-γ bands increase monotonically with ζ. The excitation energy of the 0_3^+ level is close to those of the 2_3^+ and 4_2^+ states up to $\zeta = \zeta[\mathrm{X}(5)] \approx 0.82$ and increases very rapidly for higher values of ζ.

The curves corresponding to two states of equal $J > 0$ approach each other in the region near the $[SU_{\pi\nu}(3)]$ limit. At $\zeta \simeq 0.98$ they cross, so that the states exchange their index i. An expanded view of this region is shown in the lower panel in Fig. 9. There, the symbols J_a and J_b indicate the spin of two states $|a\rangle$ and $|b\rangle$ having the same J ($J = 2$ is taken as an example). The structure of each of these states is expected to be quite the same before and after the crossing point.

The normalized energies of the 0_2^+ and 0_3^+ states, calculated for ζ[X(5)], are lower than the corresponding ones in the X(5) solution. No close correspondence of the IBA-2 states of spin $J > 0$ and index $i = 2$ or 3, for $\zeta = 0.82$, with the states of the $s = 2$ band can be noticed.

Further information on the evolution of the two bands in the whole range of ζ is obtained from the $B(E2)$ strengths and from the wave functions of some transitions of particular interest. The data concerning the $R[B(E2)]$ values are presented in Fig. 10. In the regions where the quasi-β and quasi-γ bands can be identified, the even-J states belonging to each band have the same index i because the $R[B(E2)]$ values of the $4_2^+ \to 2_3^+$, $4_3^+ \to 2_2^+$ and $6_2^+ \to 4_3^+$, $6_3^+ \to 4_2^+$ transitions are

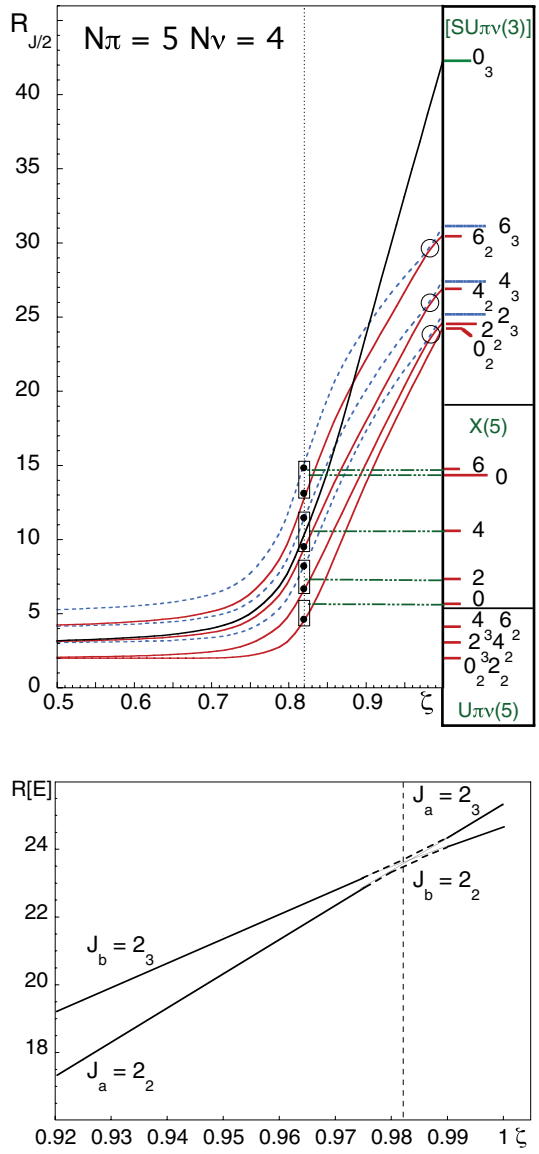

FIG. 9. (Color online) Top: Normalized excitation energies of the lowest even-J states of the quasi-β and quasi-γ bands and of the 0_3^+ state, as a function of ζ, for an $N_\pi = 5$, $N_\nu = 4$ nucleus. The corresponding values in the $U_{\pi\nu}(5)$ and $[SU_{\pi\nu}(3)]$ limits and the values of the $s = 2$ band and of the 0_{3s} state in the X(5) model are shown at the right. Solid lines represent the excitation energies of the J_i states with index $i = 2$; dashed lines, of those with index $i = 3$. The vertical line indicates the ζ[X(5)] value, whereas the circles point out the region where levels of the same $J > 0$ cross. Bottom: Expanded view of the crossing region for the 2_2^+ and 2_3^+ states.

negligible for whatever ζ. The identification of these bands is therefore based on the $B(E2; 2_2^+ \to 0_2^+)$ and $B(E2; 2_3^+ \to 0_2^+)$ values.

From the decay of the relevant transitions it turns out that in the region of $\zeta < 0.6$ the J_3 states make up the band on the 0_2^+ state. Past $\zeta \approx 0.6$ the structure of the bands starts changing, even if the excitation energies of their memberships do not vary significantly. In the approximately 0.72–0.98 range of ζ, which contains ζ[X(5)], the quasi-β band is made up of the J_2 states. At $\zeta \simeq 0.98$ the $B(E2)$ strengths of the two transitions reported in each of Figs. 10(b)–10(e) abruptly exchange their values. This is just related to the crossing of the levels of the same J, as shown in Fig. 9 for the $J = 2$ states (which does not imply significant changes in the wave functions of states $|a\rangle$ and $|b\rangle$. The indexes i of the states of the quasi-β and the quasi-γ bands therefore become the same as those of the $U_{\pi\nu}(5)$ and $[SU_{\pi\nu}(3)]$ limits. The $R[B(E2)]$ strengths of all the transitions reported in Fig. 10 are smaller, for ζ[X(5)], than the corresponding X(5) values. The curve relative to the $0_2^+ \to 2_1^+$ transition crosses the X(5) horizontal line for a value of ζ (0.80) that differs by only 2.5% from ζ[X(5)]. However, the strong slope of the curve leads to an $\simeq$30% difference in the $R[B(E2)]$ strengths. As for the other transitions, the largest differences amount to $\simeq$30% for the quasi-β band and $\simeq$50% for the quasi-γ band. A good agreement is instead obtained between the $R[B(E2; 0_3^+ \to 2_2^+)]$ and the $R[B(E2; 0_{s3}^+ \to 2_{s2}^+)]$ strengths.

Past $\zeta \simeq 0.82$ and up to $\zeta \simeq 0.98$ the normalized $B(E2)$ strengths do not change significantly. Their values could imply a structure of the bands close to the $[SU_{\pi\nu}(3)]$ limit already for $\zeta \simeq 0.82$. However, the normalized excitation energies of the two bands increase rapidly after $\zeta = 0.82$, which implies that deformation is still rapidly increasing.

The wave functions of some relevant states prove to be very useful for gaining a deeper insight into the structure of the quasi-β and quasi-γ bands along the $U_{\pi\nu}(5) \to [SU_{\pi\nu}(3)]$ transition. The n_d components of the 0_2^+, 2_2^+, and 2_3^+ states are reported in Fig. 11 for some values of ζ. For $\zeta = 0.60$ these states have a rather $U_{\pi\nu}(5)$ structure: the $n_d = 2$ component is strongly predominant for the 0_2^+ and 2_2^+ states, and the $n_d = 3$ component for the 2_3^+ state. When ζ increases, the percentages of the $n_d = 0$, 1, and 2 components in the wave functions of the 0_2^+, 2_2^+, and 2_3^+ states, respectively, start growing. They become the largest for $\zeta = 0.775$ and achieve a percentage close to 60% for ζ[X(5)] = 0.82. The structure of the states does not vary appreciably in the $\zeta \approx 0.78$–0.84 region.

For ζ[X(5)] the wave functions of the 0_2^+, 2_2^+, and 2_3^+ states are similar to those of the 0_1^+, 2_1^+, and 2_2^+ levels, respectively, of an U(5) nucleus. On the whole, the information associated with the quasi-β and quasi-γ bands suggests a vibrational structure, based on the 0_2^+ state. The main n_d components of the states of the two bands, reported in Fig. 12, have a structure (apart from the higher J_3 states) that supports this interpretation. This accounts for the fact that, in Fig. 8, the $R[E]$ curve of the quasi-β band is in a region of less deformation with respect to the corresponding X(5) curve.

The structure of the states denoted states $|a\rangle$ and $|b\rangle$ in the lower panel in Fig. 9 is shown for $\zeta = 0.975$ and $\zeta = 0.99$ in Fig. 11. It is shown that there are only small changes in their wave functions before and after $\zeta \simeq 0.98$, where the 2_2^+ and 2_3^+ states cross.

By taking into account the wave functions and the $B(E2)$ strengths of the relevant states, it is possible to understand why the composition of the quasi-β and quasi-γ bands changes upon approaching the transition region. In the low-ζ region the $2_2^+ \to 0_2^+$ transition links mainly $\Delta n_d = 0$ components, whereas in the $\zeta \approx 0.82$ region it connects predominantly

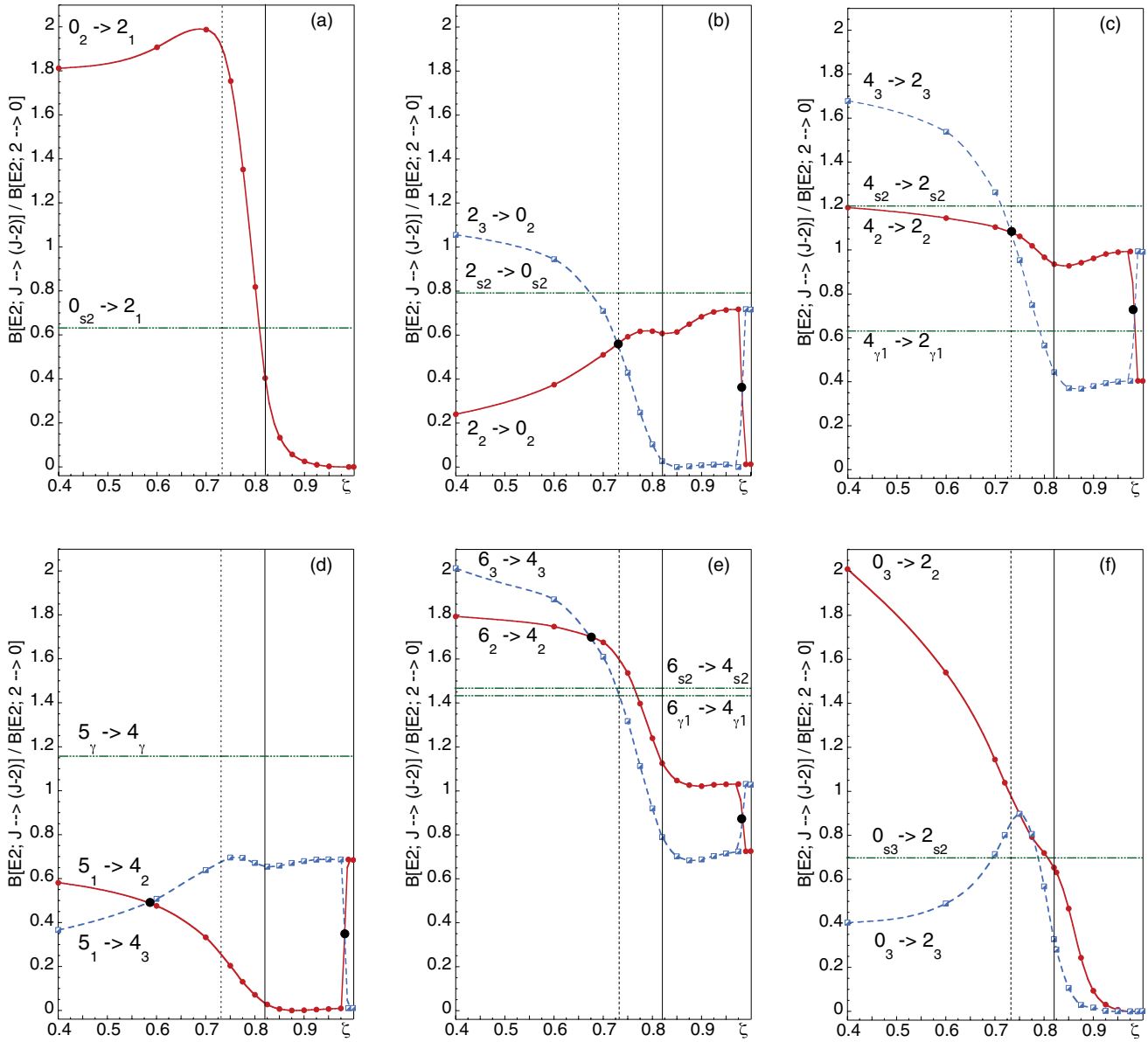

FIG. 10. (Color online) Normalized $B(E2)$ strengths of the transitions shown in each panel, as a function of ζ, for a nucleus having $N_\pi = 5$ and $N_\nu = 4$. The corresponding values predicted by the X(5) model for the $s = 2$ band and $n_\gamma = 1$ lowest band are shown as horizontal lines. The solid vertical line marks the ζ[X(5)] value; the dashed vertical line, the ζ values where the curves in (b) and (c) cross.

$\Delta n_d = 1$ components, and this gives rise to the increase in the $B(E2; 2_2^+ \to 0_2^+)$ strength. Simultaneously, the $B(E2)$ strength of the $2_3^+ \to 0_2^+$ transition, which initially links mainly $\Delta n_d = 1$ components, decreases dramatically in going towards the $\zeta \approx 0.82$ region because of the $E2$ selection rule, which forbids $\Delta n_d = 2$ transitions. For $\zeta \approx 0.82$ the quasi-β band is thus made up of J_2 states.

In the $\zeta \approx 0.78$–0.84 region, where the structure of the states does not change appreciably, the $R[B(E2; 2_2^+ \to 0_2^+]$ strength has a constant value, smaller than the $[\mathrm{SU}_{\pi\nu}(3)]$ one, achieved for higher ζ.

The coexistence of vibrational and rotational motions, which results from the data presented up to now, is also evident from the data in Fig. 13. There, the $R[E]$ values of the g.s. band and the excitation energies of the quasi-β band, normalized to that of the 2^+ member of the band, are reported, as a function of J, for ζ[X(5)]. The deformation of the excited band is smaller than that of the g.s. band. These findings are in agreement with global experimental data (see, e.g., Fig. 4 in Ref. [41]).

The excitation energy and decay patterns of the states considered until now are displayed in Fig. 14 for some value of ζ of particular interest. For $\zeta = 0.4$ the nuclear structure is close to that of the $\mathrm{U}_{\pi\nu}(5)$ limit, with multiplets clearly visible and strong $E2$ transitions connecting states of subsequent multiplets. For $\zeta = 0.75$, i.e., in the region where the curves in Figs. 10(b) and 10(c) first cross, the states belonging to the multiplets start splitting, with couplets of states (3_1, 4_2 and 4_3, 5_1), still close in energy. The 0_3 states decays to both the 2_2 and the 2_3 states. For ζ[X(5)] ≈ 0.82 the structure of the quasi-β and quasi-γ bands is not far from that of an anharmonic vibrator. To

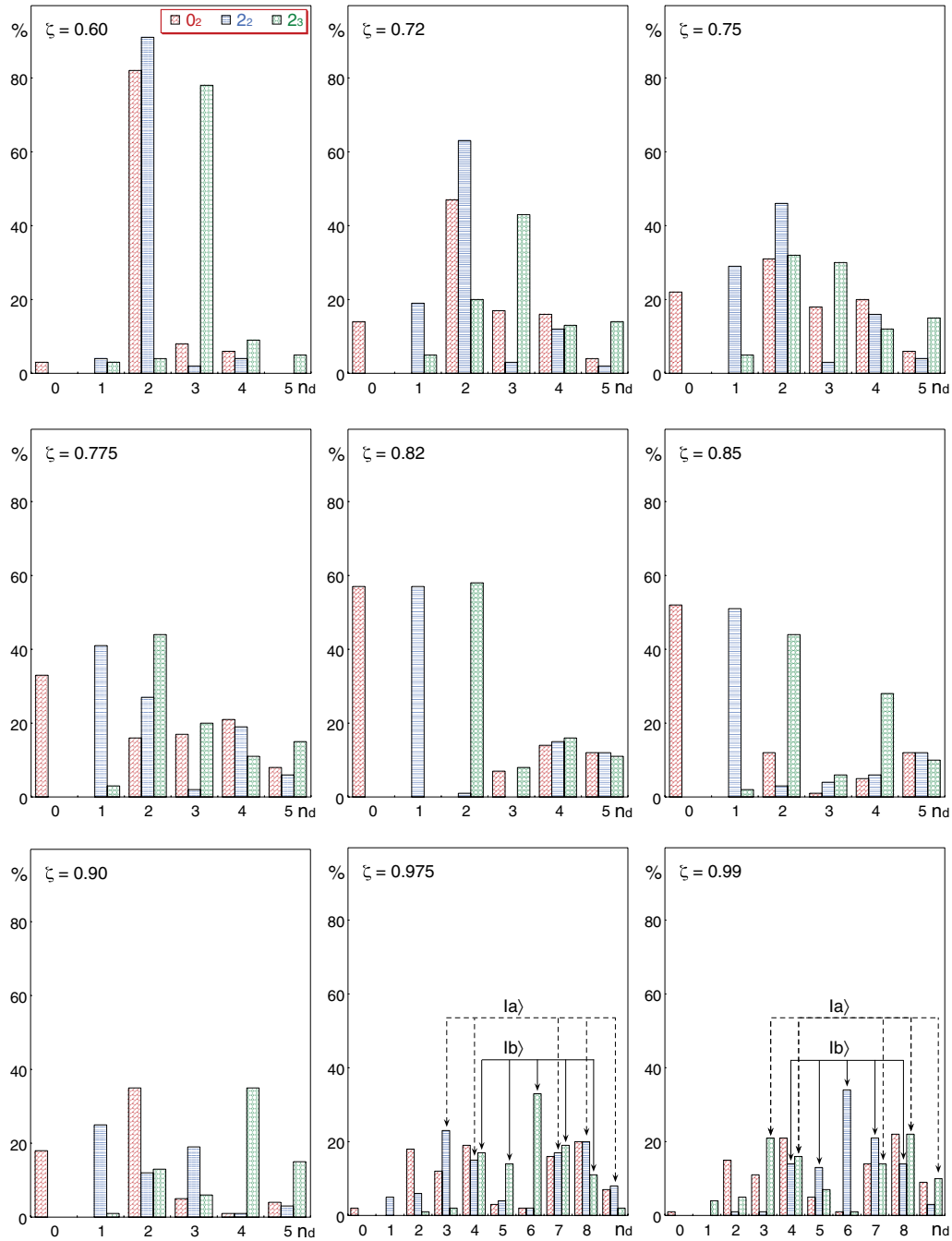

FIG. 11. (Color online) Percentage of the n_d components of the 0_2^+, 2_2^+, and 2_3^+ states for some values of ζ of particular interest in the evolution of quasi-β and quasi-γ bands. In the panels corresponding to $\zeta = 0.975$ and $\zeta = 0.99$ the arrows indicate the largest components of the states, denoted as states $|a\rangle$ (dashed lines) and $|b\rangle$ (solid lines) in the lower panel in Fig. 9.

stress this point the 8_2^+ level has been included in the panel and the states of the two quasibands have been inserted in a dotted rectangle. The normalized $B(E2)$ strengths of the $0_3^+ \to 2_1^+$ and $0_3^+ \to 2_2^+$ transitions (0.005 and 0.65, respectively) are rather close to those predicted by the X(5) model (0.001 and 0.85, respectively). Upon going from ζ[X(5)] to $\zeta = 1$ the quasi-β and quasi-γ bands move to very high excitation energies with respect to the g.s. band and attain the structure predicted by the [$SU_{\pi\nu}(3)$] limit for the β and γ bands.

III. COMPARISON OF IBA-2 AND X(5) PREDICTIONS WITH EXPERIMENTS

From the data presented in Sec. II it turns out that IBA-2 results can differ appreciably from the predictions of the macroscopic X(5) model when the calculated quantities depend on the boson number and N_B is small. In this section the predictions of two models are compared to the experimental data on even neodymium ($N > 82$) isotopes [42]. This isotopic chain has a structure which changes from spherical to axially

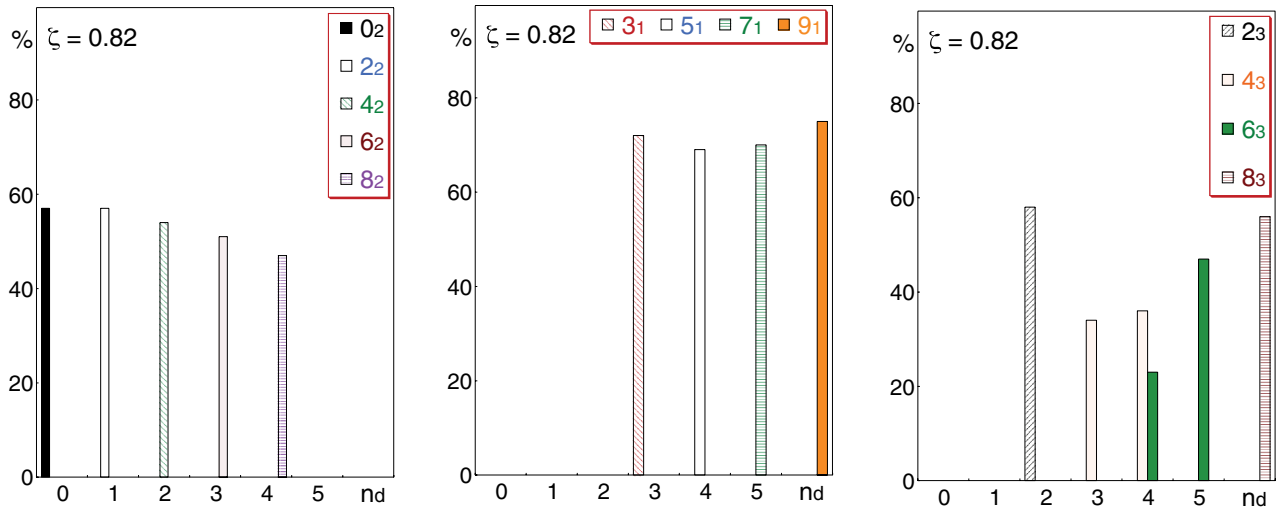

FIG. 12. (Color online) Percentage of the major n_d component(s) of the states of the quasi-β band (left) and of the odd-J states (center) and even-J states (right) of the quasi-γ bands, for $\zeta = 0.82$.

symmetric for increasing A and contains the ^{150}Nd isotope, considered one of the best examples of an X(5)-like nucleus. The spectroscopic properties of the $^{144-156}$Nd isotopes ($N_\pi = 5$, $N_\nu = 1$–7) concerning excitation energies, dipole and quadrupole moments, $E2$ and $M1$ transition strengths, and branching ratios have recently been investigated [29,43]

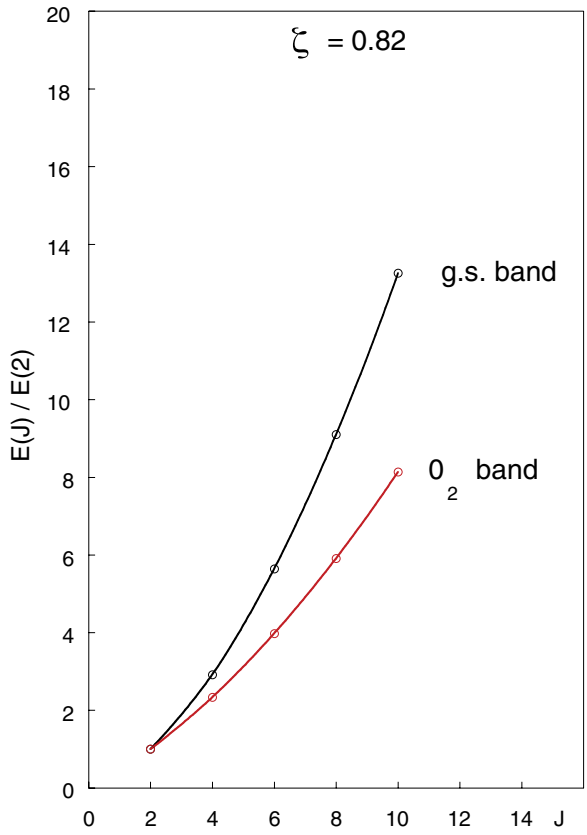

FIG. 13. (Color online) Normalized excitation energies, as a function of J, of the g.s. band and the quasi-β bands, for $\zeta = 0.82$.

in the framework of the IBA-2 model. The calculations have been carried out using the Hamiltonian

$$H = \varepsilon\left(\hat{n}_{d_\pi} + \hat{n}_{d_\nu}\right) + \kappa\, \hat{Q}_\pi^{(\chi_\pi)} \cdot \hat{Q}_\nu^{(\chi_\nu)} + \hat{M}_{\pi\nu}, \qquad (8)$$

where $\hat{M}_{\pi\nu}$ is the generalized Majorana operator [38].

Both parameters χ_π and χ_ν have been kept equal to the value $-\sqrt{7}/2$. The values deduced for the Hamiltonian parameters are reported in Table I. An overall good agreement with the experimental data was achieved by considering states of FS as well as of MS character. It turned out that all the states belonging to the g.s. bands and to the band built on the 0_2^+ state in ^{150}Nd (the only band built on an excited 0^+ state identified in the isotopic chain) are FS. The symmetry character of the 2_3^+ and 3_1^+ states, which is predominantly MS in $^{144-148}$Nd isotopes, changes abruptly in ^{150}Nd, where the FS components of the wave functions are larger than 95%. These findings make it possible to exclude from the analysis states like the 2_3^+ and 3_1^+ ones in $^{144-1148}$Nd. The fact that their energy regularly increases with A (see Fig. 12 in Ref. [29]) could erroneously suggest an interpretation in terms of the lowest members of the quasi-β and quasi-γ bands. In addition, the knowledge of the symmetry character of the relevant states allows one to limit the study to the states of FS character. In such a case the Majorana term can be neglected in Hamiltonian (8), which can thus be expressed in a form similar to Hamiltonian (6) by performing the proper renormalization, $\zeta = 4N_B/(4N_B + \varepsilon/\kappa)$; see, e.g., [44]. The ζ values used in the present calculations are deduced from parameters ϵ and κ of Ref. [29] and are reported in the last column in Table I.

The change in structure along the neodymium chain is apparent in Fig. 15, where the experimental $R_{4/2}$ values of $^{144-156}$Nd are shown as a function of the values of ζ given in Table I. The anomalous value of ^{144}Nd is caused by the presence of noncollective components in the wave functions of the 4_1^+ state [43,45]. The ^{150}Nd isotope was first identified by Casten and Zamfir [15] as an X(5)-like nucleus on the basis of the energy spacing of the yrast states, in nearly perfect

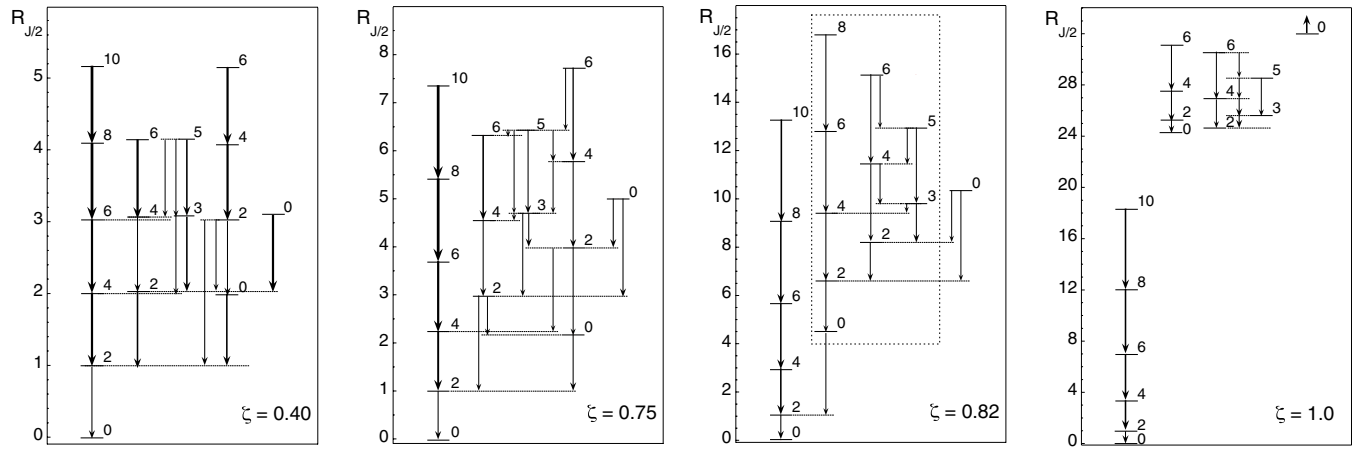

FIG. 14. Excitation energy patterns of an $N_\pi = 5$, $N_\nu = 4$ nucleus, for the values of ζ reported in each panel. The thickness of the arrows indicates the normalized $B(E2)$ strengths. Only transitions having $R[B(E2)]$ values larger than 0.5 are shown. In the panel corresponding to $\zeta = 0.82$ a dotted rectangle including the states belonging to the quasi-β and quasi-γ bands is drawn.

agreement with the model predictions. The normalized $B(E2)$ strengths of the transitions de-exciting the $J \leqslant 10$ yrast levels, measured in Ref. [16], were also found to be close to the X(5) values, apart from the $B(E2; 10_1^+ \rightarrow 8_1^+)$ value. The agreement was not as good for the $s = 2$ band.

The experimental excitation energies of the g.s. band and of the 0_2^+ band in ^{150}Nd, reported as a function of J, are compared to the X(5) predictions and to the IBA-2 values in Fig. 16, where the predictions of the $U_{\pi\nu}(5)$ and $[SU_{\pi\nu}(3)]$ limits are also shown. The IBA-2 values reproduce the excitation energies of the g.s. band satisfactorily, even though not as well as the X(5) model. Instead they match the energies of the 0_2^+ band better. It is to be remarked that this band is made up of J_i states having index $i = 2$, as expected on the basis of the results presented in Sec. II.

The comparison for the normalized $B(E2)$ strengths of the g.s. band and of the quasi-β band in ^{150}Nd are shown in Fig. 17. The experimental values of the g.s band [16,42,46] include additional data with respect to those considered in Ref. [16].

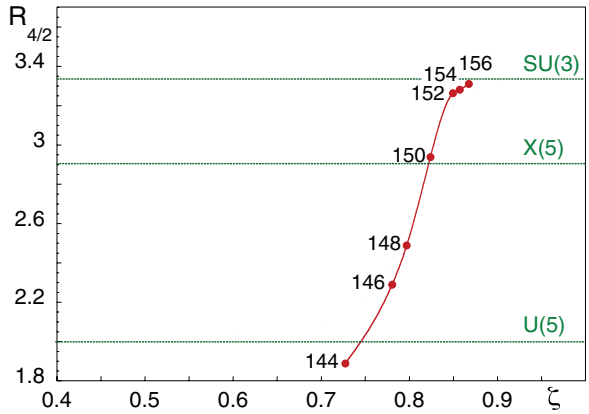

FIG. 15. (Color online) Experimental $R_{4/2}$ values of heavy neodymium isotopes reported as a function of the values of ζ listed in Table I. Horizontal lines indicate the corresponding U(5), X(5), and SU(3) values.

The $R[B(E2)]$ strengths predicted by the IBA-2 model for the g.s. band are close to the experimental data, whereas the X(5) values turn away for increasing J. A close comparison of IBA-2 and X(5) predictions for the normalized $B(E2)$ values of the quasi-β band is hampered by the large errors affecting the experimental data, except for the $B(E2; 0_2^+ \rightarrow 2_1^+)$ strength. In this case the IBA-2 value is closer to the experimental one than the X(5) one.

As for the quasi-γ band, only two possible members are known, i.e., the 2_3^+ and 3_1^+ states, however, the $E2$ transition strengths of the de-exciting transitions have not yet been measured. The energies of these states are reproduced to better than 5% in Ref. [29]. For additional tests of the findings in Sec. II, the experimental data concerning excitation energies and $E2$ transition probabilities of the g.s. bands in $^{146-156}$Nd isotopes and in $N = 90$ isotones are taken into account.

In the top panel in Fig. 18 the experimental $R[E]$ values of the levels of neodymium isotopes (identified as states of collective nature in Ref. [29]) are reported, as a function of J, together with the U(5), SU(3), and X(5) predictions. The values of $^{146-148}$Nd are not far from that of the U(5) limit, while those of $^{152-156}$Nd gather near the SU(3) limit. The ^{150}Nd is in an outstanding position, as expected for a nucleus close to the critical point of a phase transition. No

TABLE I. Values of the Hamiltonian parameters deduced in the analysis of even $^{144-156}$Nd isotopes in Ref. [29] are reported (in MeV) in columns 2–5 (those kept fixed are in italics). In the last column we give the value of ζ deduced, for each isotope, from ϵ and $\kappa_{\pi\nu}$.

A	ε	$\kappa_{\pi\nu}$	ξ_2	ξ_3	ζ
144	0.900	−0.100	0.350	−0.350	0.73
146	0.850	−0.108	0.150	−0.350	0.78
148	0.750	−0.092	0.080	−0.300	0.80
150	0.500	−0.065	0.060	−0.300	0.82
152	0.390	−0.055	*0.500*	*0.500*	0.85
154	0.425	−0.058	*0.500*	*0.500*	0.86
156	0.440	−0.060	*0.500*	*0.500*	0.87

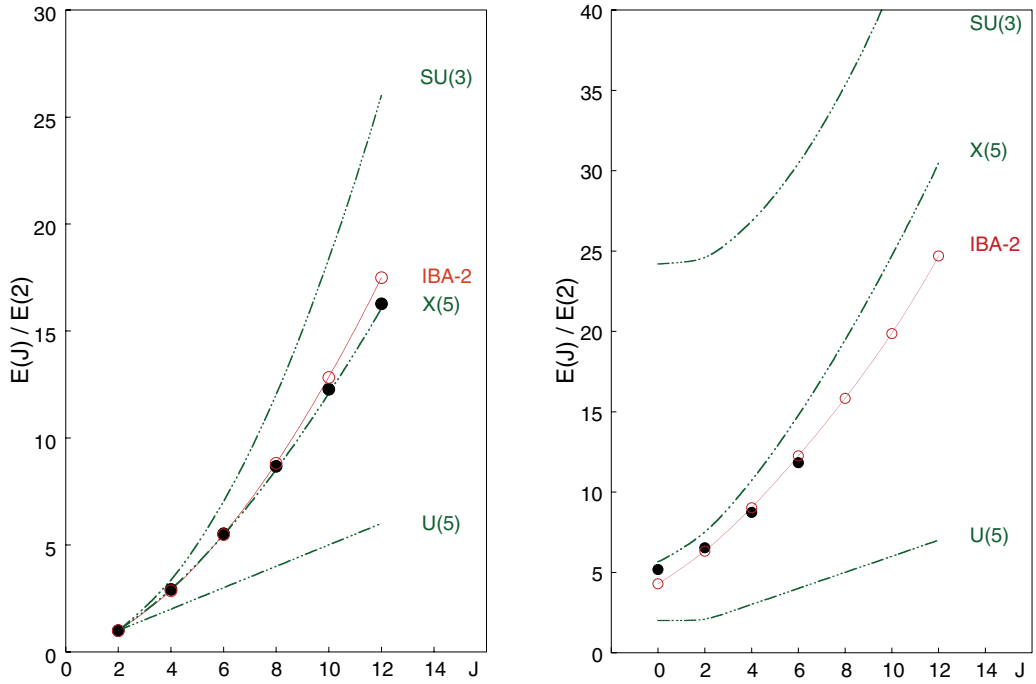

FIG. 16. (Color online) Left: Experimental (filled circles) energies of the g.s. band in ^{150}Nd compared to the U(5), X(5), and SU(3) predictions (dashed lines) and to the results of the IBA-2 calculations [29] (open circles). Right: Experimental (filled circles) normalized energies of states belonging to the 0_2^+ band compared to the values predicted (dashed lines) by the X(5) model for the $s = 2$ band, those predicted by the SU(3) and U(5) limit for the band on the 0_2^+ state, and the results of the IBA-2 calculations [29] (open circles).

such peculiar behavior is instead displayed by the normalized $B(E2)$ values, as shown in the bottom panel in Fig. 18. Here, the data concerning $^{148-152}$Nd ($N_B = 8$–10) are reported, as a function of J, together with the predictions of the U(5) and SU(3) limits for $N_B = 9$. These isotopes are the only ones among the heavy neodymium isotopes where the trend of the experimental values can be clearly observed. It is shown that the values of ^{148}Nd are as close to the SU(3) limit as those of ^{150}Nd and this is in contrast to the conclusions one could draw from the top panel in the figure.

The experimental $R[E]$ and $R[B(E2)]$ values of the g.s. bands in $N = 90$ isotones [42] are reported, as a function of J, in Fig. 19. By looking at the $R[E]$ values it appears that ^{152}Sm and ^{154}Gd are more deformed than ^{150}Nd. However, as shown in the bottom panel, the $B(E2)$ strengths of ^{150}Nd are closer to the SU(3) values than those of the heavier isotones, which instead approach the X(5) values. This is just what is expected on the basis of the data presented in Fig. 4.

The data on the normalized excitation energies and $B(E2)$ strengths of the g.s. band in these isotopic and isotonic chains

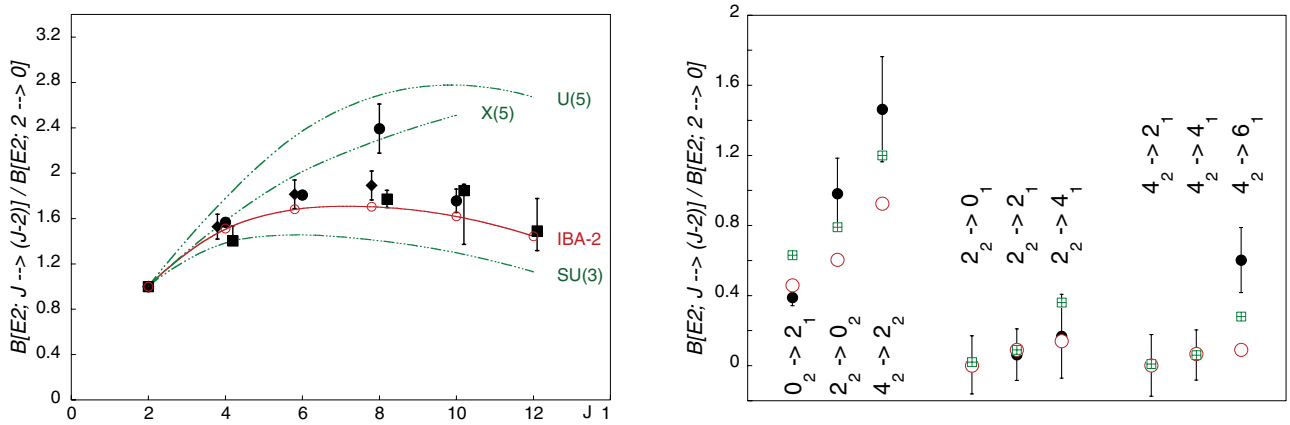

FIG. 17. (Color online) Left: Experimental $B(E2)$ ratios of the g.s. band in ^{150}Nd compared to the predictions (dashed lines) of the X(5) model and of the U(5) and SU(5) limits (for $N_B = 9$) and to the IBA-2 results (open circles). Experimental values are from Refs. [42] (filled diamonds), [16] (filled circles), and [46] (filled squares). Right: Experimental $B(E2)$ ratios [16] of the quoted transitions in ^{150}Nd compared to the X(5) predictions (crossed open squares) and to the results of the IBA-2 calculations (open circles).

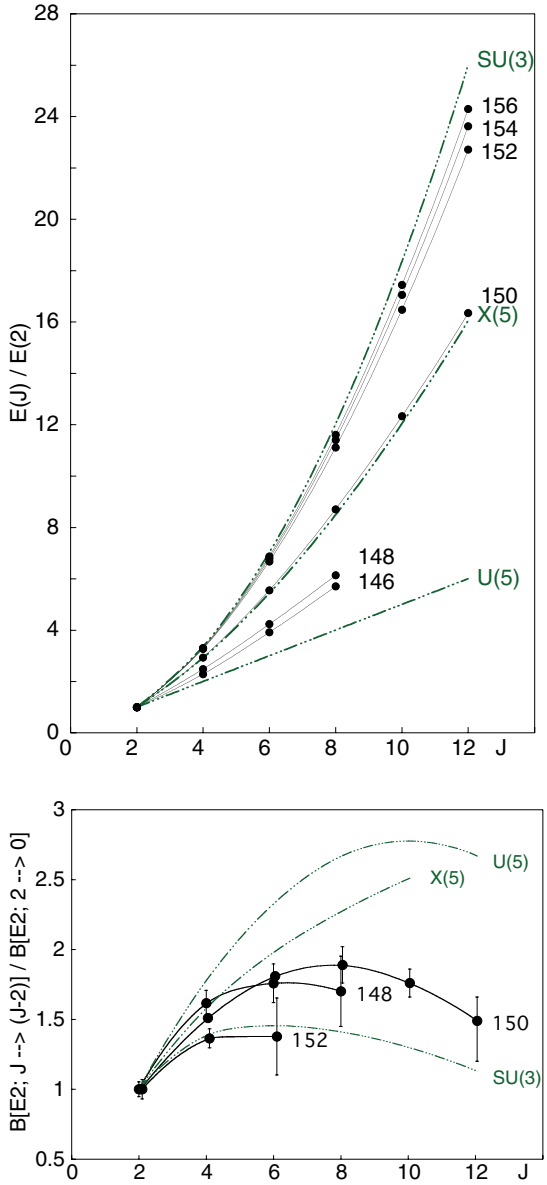

FIG. 18. (Color online) Top: Experimental normalized energies of the g.s. band in $^{146-156}$Nd isotopes. Bottom: Experimental $B(E2)$ ratios of the g.s. band in $^{148-152}$Nd; the data on ^{148,152}Nd are from Ref. [42]; those on ^{150}Nd are the weighted averages of the data reported in Refs. [16,42], and [46]. In both panels the predictions (dotted-dashed line) of the X(5) model and of the U(5) and SU(3) limits for $N_B = 9$ are also shown.

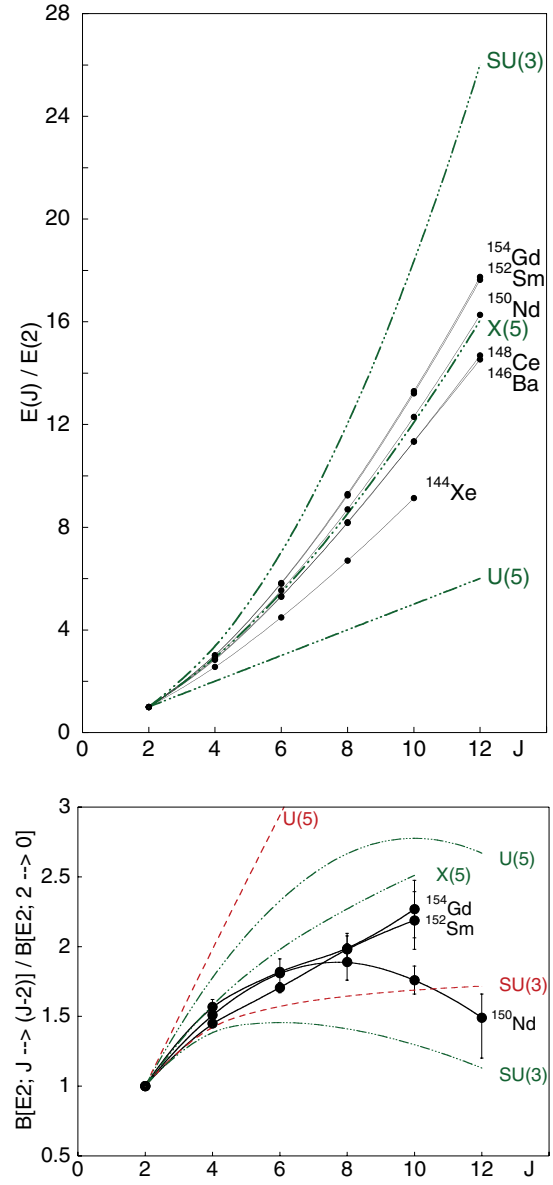

FIG. 19. (Color online) Top: Experimental normalized energy of the g.s. band in $N = 90$ isotones shown together with the predictions (dashed lines) of the X(5) model and of the U(5) and SU(3) symmetries. Bottom: Experimental $B(E2)$ ratios of the g.s. band in $N = 90$ Nd, Gd, and Sm isotones shown together with the predictions of the X(5) model and of the U(5) and SU(3) limits for $N_B = 9$ (dotted-dashed lines) and for large N_B (dashed lines). Experimental data are from Ref. [42].

support the findings of Sec. II about the importance of taking into account the finite number of bosons to achieve a correct description of the experimental data and about the possibility that the IBA description approaches the X(5) one for a large boson number.

Further information about the structure evolution of the Nd chain can be obtained from the n_d components of g.s. wave functions in $^{144-156}$Nd, calculated with the parameters of Ref. [29]. The percentage of the main components in each isotope is shown in Fig. 20. The ^{144}Nd isotope has a structure very close to that of the U(5) limit. The $n_d = 0$ component is predominant in ^{146}Nd and still has a percentage larger than 50% in ^{148}Nd, whereas the $n_d = 2$ is the main component in ^{150}Nd. In the heavier isotopes n_d components of comparable intensities are present with a large range of values, as expected for nuclei approaching the SU(3) limit. From these data, ^{148}Nd seems to be the isotope closest to the transition point, even if, in this case, a clear statement on which to base the identification is missing.

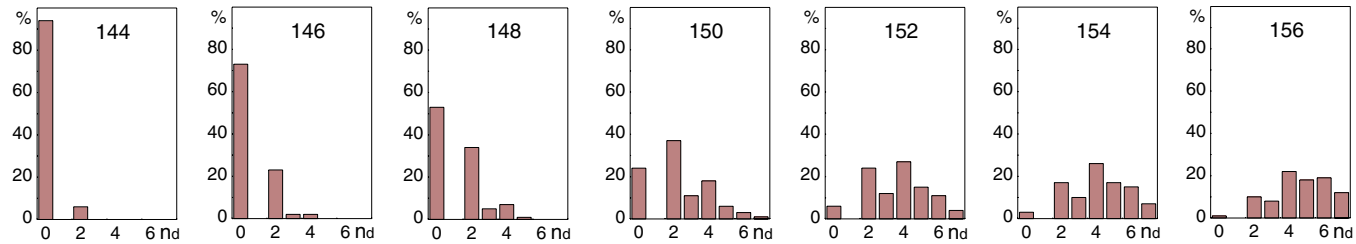

FIG. 20. (Color online) Percentage of the n_d components in the ground state of heavy Nd isotopes, evaluated in the IBA-2 model using the parameters of Ref. [29].

IV. PES CALCULATIONS IN THE IBA-2 MODEL FOR NEODYMIUM-144–156

Additional information on the structure of heavy Nd isotopes and on the possible identification of ^{150}Nd as an X(5)-like nucleus can be obtained from the study of the g.s. PESs performed through the coherent-state formalism [30–32]. In the IBA-2 model one has to consider two fluids and their mutual interaction according to Hamiltonian (4). The PESs can be obtained by calculating matrix elements of the Hamiltonian within intrinsic coherent states that separate the proton and neutron contribution, defined as

$$|N_\pi, N_\nu, \beta_\pi, \beta_\nu, \gamma_\pi, \gamma_\nu; \text{g.s.}\rangle = \frac{1}{\sqrt{N_\pi! N_\nu!}} (B_\pi^\dagger)^{N_\pi} (B_\nu^\dagger)^{N_\nu} |0\rangle. \quad (9)$$

This expression is shortened to $|\text{g.s.}\rangle$ in the following. The boson creator operators of each species are defined as a linear combination of the basic s and d_μ operators as

$$B_\rho^\dagger = \frac{1}{\sqrt{1+\beta_\rho^2}} \left(s_\rho^\dagger + \beta_\rho \cos(\gamma_\rho) d_{0\rho}^\dagger + \beta_\rho \frac{\sin(\gamma_\rho)}{\sqrt{2}} (d_{2\rho}^\dagger + d_{-2\rho}^\dagger) \right). \quad (10)$$

The expectation value of $\hat{Q}_\pi \cdot \hat{Q}_\nu$ in the g.s. is

$$\begin{aligned} &\langle \text{g.s.}|\hat{Q}_\pi \cdot \hat{Q}_\nu|\text{g.s.}\rangle \\ &= \frac{2 N_\pi N_\nu \beta_\pi \beta_\nu}{7(1+\beta_\pi^2)(1+\beta_\nu^2)} \\ &\quad \times (14 \cos(\gamma_\pi - \gamma_\nu) + \chi_\pi \chi_\nu \beta_\pi \beta_\nu \cos(2\gamma_\pi - 2\gamma_\nu) \\ &\quad - \sqrt{14}(\chi_\pi \beta_\pi \cos(2\gamma_\pi + \gamma_\nu) + \chi_\nu \beta_\nu \cos(\gamma_\pi + 2\gamma_\nu))). \end{aligned} \quad (11)$$

Note that it differs from Eq. (2.12) in Ref. [7] in the sign in front of the last term.[1]

The expectation value for the Maiorana operator $\hat{M}_{\pi\nu}$ [48], within g.s. coherent states, is given by

$$\begin{aligned} &\langle \text{g.s.}|\hat{M}_{\pi\nu}|\text{g.s.}\rangle \\ &= \frac{N_\pi N_\nu \beta_\pi \beta_\nu}{2(1+\beta_\pi^2)(1+\beta_\nu^2)} \big(\xi_2(\beta_\pi^2 + \beta_\nu^2) \\ &\quad - 2\xi_2 \beta_\pi \beta_\nu \cos(\gamma_\pi - \gamma_\nu) - \xi_3 \beta_\pi^2 \beta_\nu^2 \sin(\gamma_\pi - \gamma_\nu)^2\big). \end{aligned} \quad (12)$$

It reduces to Eq. (2.13) of Ref. [7] when $\xi_1 = \xi_3 = -2$ and $\xi_2 = 2$. Note the absence of terms with ξ_1 in the g.s. and also that Eq. (12) gives 0 for $\beta_\pi = \beta_\nu$ and $\gamma_\pi = \gamma_\nu$. Therefore the Majorana operator affects the g.s. PESs only if some imbalance is chosen between the deformations and the asymmetry angle of the proton and neutron fluids. It is noteworthy that the largest effects are expected for isotopes that have neutron and proton bosons in different shells or that occupy the same (large) shell in a very dissimilar way.

Contour plots of PESs for Hamiltonian (8) are given in Fig. 21 for even $^{144-156}$Nd, taking $\gamma_\pi = \gamma_\nu$ for simplicity. The parameters are the ones given in Table I and Ref. [29] ($\chi_\pi = \chi_\nu = -\sqrt{7/2}$). The Majorana term is included, although its contribution is almost negligible (see, e.g., Fig. 22 to appreciate the change). The horizontal and vertical axes are labeled β_π and β_ν, respectively. These figures show that, while ^{144}Nd and ^{146}Nd have a clear spherical minimum, the isotopes $^{150-156}$Nd have a clear prolate deformed minimum. The case of ^{148}Nd is very close to the critical point, lying slightly toward the deformed side. Sections of the potential energies in Fig. 21 are given in Fig. 22 as a function of β taken along the line connecting the origin with the absolute minimum, again with $\gamma_\pi = \gamma_\nu = 0$. This figure shows that the minimum for ^{148}Nd is already at some non-null value of β.

V. CONCLUSIONS

The $\text{U}_{\pi\nu}(5) \to [SU_{\pi\nu}(3)]$ transition is investigated in the framework of the IBA-2 model using a one-parameter (ζ) Hamiltonian. This is the only parameter varied in the analysis, as the effects of effective charges on normalized $B(E2)$ reduced transition strengths are negligible.

The normalized excitation energies and $B(E2)$ strengths of the g.s., quasi-β, and quasi-γ bands are studied as a function of ζ. The results obtained for the value of ζ

[1]The authors of Ref. [7] agree that there was a misprint in Ref. [7].

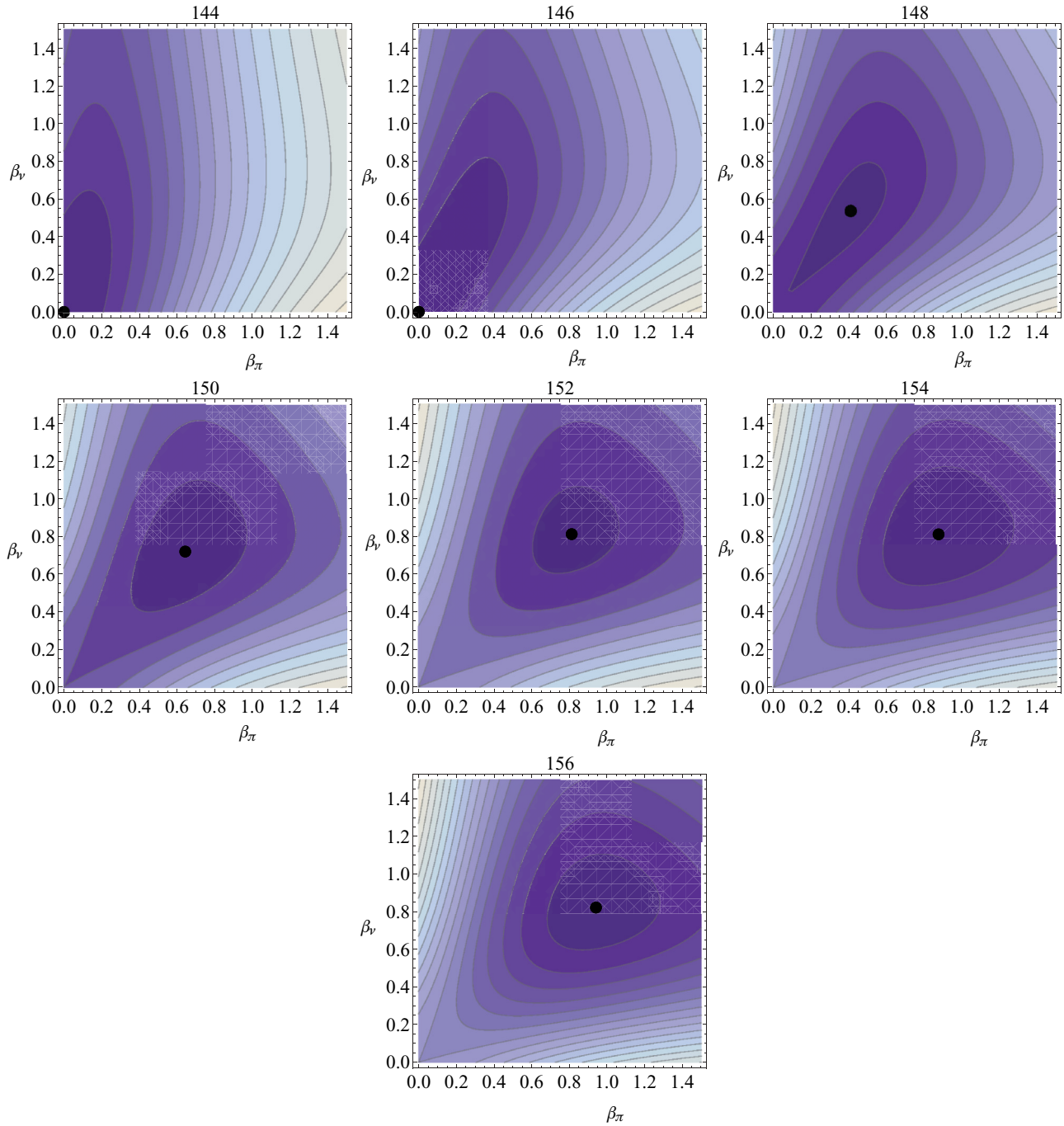

FIG. 21. (Color online) Contour plots of ground-state potential energy surfaces calculated with Hamiltonian (8), *including* the Majorana term, as a function of β_π and β_ν, for even $^{144-156}$Nd isotopes. The values of β_π and β_ν as well as of χ_π and χ_ν are irrelevant for the cases with a spherical minimum ($A \leqslant 146$), while they correspond to prolate values for all other isotopes. The parameters ϵ, κ, ξ_2, and ξ_3 are listed in Table I. The darkest color corresponds to the minimum, which is also marked by a filled (black) circle.

which leads to $R_{4_1/2_1} = 2.91$ are compared to the X(5) predictions. Noticeable differences are found in the $R[B(E2)]$ strengths for a finite boson number, which decrease as N_B increases.

A detailed analysis of the evolution of the quasi-β and quasi-γ bands is performed for an $N_\pi = 5$, $N_\nu = 4$ nucleus, also taking into account the wave functions of the relevant states. It turns out that for $\zeta[\mathrm{X}(5)]$ the two bands have, on the whole, a quite anharmonic vibrational structure, with the 0_2^+ state as band head.

The predictions of the IBA-2 and X(5) models are tested by referring to the experimental data concerning even Nd ($N > 82$) isotopes and the $N = 90$ isotonic chain. Both include the X(5)-like nucleus ^{150}Nd, which has $N_\pi = 5$ and

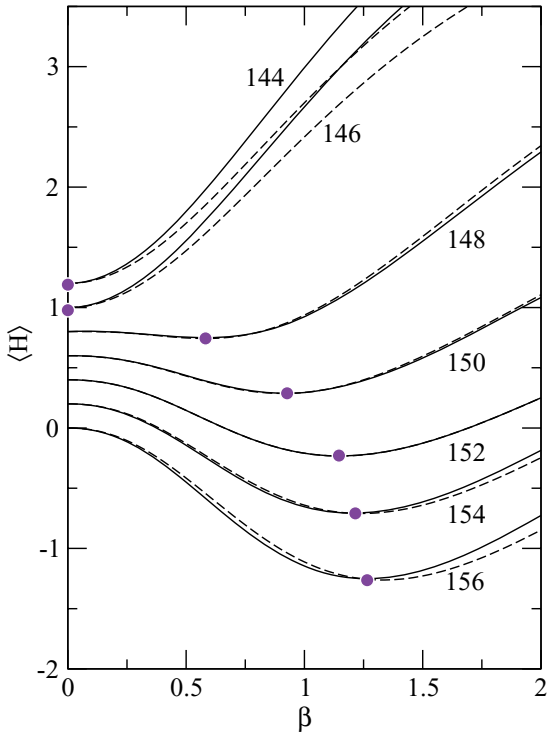

FIG. 22. (Color online) Cuts of the PESs for neodymium isotopes: along the x axis for ^{144,146}Nd and along the line connecting the origin to the minimum (see Fig. 21) for all other cases. Vertical values have been shifted in order to allow easier comparison. The position of the minimum is indicated by a filled circle. The effects of the Majorana term are small in all instances.

$N_\nu = 4$. The IBA-2 calculations correctly describe ^{150}Nd, also reproducing the $R[B(E2)]$ values of the g.s. band and the $R[E]$ values of the quasi-β band, overestimated by the X(5) model. It is to be remarked that the X(5) model allows one to immediately identify the small region around ζ[X(5)] where the properties of the quasi-β and quasi-γ bands change rather suddenly, giving rise to the anharmonic aforementioned structure.

The wave functions of the g.s. in the Nd chain, calculated with the parameters of Ref. [29], show that ^{148}Nd has an $U_{\pi\nu}(5)$-$SU_{\pi\nu}(3)$ intermediate structure.

Further information on the structure evolution along the neodymium chain is obtained via PES calculations, performed in the framework of the IBA-2 model with the parameters of Ref. [29]. A prolate deformed minimum is already present in $A \approx 148$, so that apparently ^{148}Nd would be the closest isotope to the critical point. Of course this kind of calculation should be taken only as an indication of the fact that both ^{148}Nd and ^{150}Nd are very close to the critical point and perhaps neither of them is sitting precisely on top of it.

Recent microscopic calculations for neodymium isotopes performed with a self-consistent relativistic mean-field approach [49] and a relativistic mean-field + BCS approach [50,51] are in agreement with our conclusions. Figure 4 in Ref. [49] and Fig. 1 in Ref. [51] show that a configuration with two minima, albeit very shallow ones, is already present in ^{148}Nd and becomes more pronounced in ^{150}Nd. Within the microscopic approaches, we have to mention, finally, the calculations of Ref. [52], based on the beyond-mean-field approximation combined with the Gogny interaction. Although their results are qualitatively consistent with the other microscopic approaches, the authors of Ref. [52] strongly question the interpretation of shape changes as nuclear shape phase transitions.

ACKNOWLEDGMENT

We thank P. Sona for fruitful discussions.

[1] F. Iachello and A. Arima, *The Interacting Boson Model* (Cambridge University Press, Cambridge), and references therein.
[2] J. N. Ginocchio and M. W. Kirson, Phys. Rev. Lett. **44**, 1744 (1980).
[3] A. E. L. Dieperink, O. Scholten, and F. Iachello, Phys. Rev. Lett. **44**, 1747 (1980).
[4] J. M. Arias, J. E. Garcia-Ramos, and J. Dukelsky, Phys. Rev. Lett. **93**, 212501 (2004).
[5] M. A. Caprio and F. Iachello, Phys. Rev. Lett. **93**, 242502 (2004).
[6] M. A. Caprio, Phys. Rev. C **69**, 044307 (2004).
[7] M. A. Caprio and F. Iachello, Ann. Phys. **318**, 454 (2005).
[8] M. A. Caprio, Phys. Rev. C **72**, 054323 (2005).
[9] A. Arima, T. Otsuka, F. Iachello, and I. Talmi, Phys. Lett. B **66**, 205 (1977).
[10] T. Otsuka, A. Arima, and F. Iachello, Nucl. Phys. A **309**, 1 (1978).
[11] F. Iachello, Phys. Rev. Lett. **87**, 052502 (2001).
[12] F. Iachello, Phys. Rev. Lett. **85**, 3580 (2000).
[13] A. Bohr and B. R. Mottelson, *Nuclear Structure* (Benjamin, New York, 1975).
[14] R. Bijker, R. F. Casten, N. V. Zamfir, and E. A. McCutchan, Phys. Rev. C **68**, 064304 (2003).
[15] R. F. Casten and N. V. Zamfir, Phys. Rev. Lett. **87**, 052503 (2001).
[16] R. Krücken *et al.*, Phys. Rev. Lett. **88**, 232501 (2002).
[17] R. M. Clark *et al.*, Phys. Rev. C **68**, 037301 (2003), and references therein.
[18] R. F. Casten, N. V. Zamfir, and R. Krücken, Phys. Rev. C **68**, 059801 (2003).
[19] A. Dewald *et al.*, Eur. Phys. J. A **20**, 173 (2004).
[20] D. Tonev *et al.*, Phys. Rev. C **69**, 034334 (2004).
[21] C. Fransen, N. Pietralla, A. Linnemann, V. Werner, and R. Bijker, Phys. Rev. C **69**, 014313 (2004).
[22] E. A. McCutchan *et al.*, Phys. Rev. C **69**, 024308 (2004).
[23] E. A. McCutchan, N. V. Zamfir, R. F. Casten, M. A. Caprio, H. Ai, H. Amro, C. W. Beausang, A. A. Hecht, D. A. Meyer, and J. J. Ressler, Phys. Rev. C **71**, 024309 (2005).
[24] D. l. Balabanski *et al.*, Int. J. Mod. Phys. E **15**, 1735 (2006).
[25] E. A. McCutchan *et al.*, Phys. Rev. C **73**, 034303 (2006).
[26] O. Möller *et al.*, Phys. Rev. C **74**, 024313 (2006).

[27] A. F. Mertz *et al*., Phys. Rev. C **77**, 014307 (2008).
[28] P. G. Bizzeti *et al*., Phys. Rev. C **82**, 054311 (2010).
[29] A. Giannatiempo, Phys. Rev. C **84**, 024308 (2011).
[30] R. Gilmore, C. M. Bowden, and L. M. Narducci, Phys. Rev. A **12**, 1019 (1975).
[31] R. Gilmore, J. Math. Phys. **20**, 891 (1979).
[32] W. Zhang, D. H. Feng, and R. Gilmore, Rev. Mod. Phys. **62**, 867 (1990).
[33] E. A. McCutchan, N. V. Zamfir, and R. F. Casten, Phys. Rev. C **71**, 034309 (2005).
[34] D. D. Warner and R. F. Casten, Phys. Rev. C **28**, 1798 (1983).
[35] P. O. Lipas, P. Toivonen, and D. D. Warner, Phys. Lett. B **155**, 295 (1985).
[36] G. Rosensteel and D. J. Rowe, Nucl. Phys. A **759**, 92 (2005).
[37] R. F. Casten, in *Interacting Bose-Fermi Systems in Nuclei*, edited by F. Iachello (Plenum Press, New York, 1981), p. 3.
[38] I. Talmi, *Simple Models of Complex Nuclei* (Harwood Academic, Basel, 1993).
[39] T. Otsuka and N. Yoshida, Program NPBOS Japan Atomic Energy Research Institute Report JAERI-M85-094 (1985).
[40] A. Arima and F. Iachello, Ann. Phys. (NY) **111**, 201 (1978).
[41] D. Bonatsos, E. A. McCutchan, N. Minkov, R. F. Casten, P. Yotov, D. Lenis, D. Petrellis, and I. Yigitoglu, Phys. Rev. C **76**, 064312 (2007).
[42] NNDC database, http://nndc.bnl.gov.
[43] A. Giannatiempo, Phys. Rev. C **84**, 034319 (2011).
[44] R. F. Casten, Nature Phys. **2**, 811 (2006).
[45] J. Holden *et al*., Phys. Rev. C **63**, 024315 (2001).
[46] M. Zielinska, Int. J. Mod. Phys. E **13**, 71 (2004).
[47] M. Caprio, private communication (April 2010).
[48] A. Giannatiempo, A. Nannini, and P. Sona, Phys. Rev. C **58**, 3316 (1998).
[49] R. Fossion, D. Bonatsos, and G. A. Lalazissis, Phys. Rev. C **73**, 044310 (2006).
[50] T. Niksic, D. Vretenar, G. A. Lalazissis, and P. Ring, Phys. Rev. Lett. **99**, 092502 (2007).
[51] Z. P. Li, T. Niksic, D. Vretenar, J. Meng, G. A. Lalazissis, and P. Ring, Phys. Rev. C **79**, 054301 (2009).
[52] T. R. Rodriguez and J. L. Egido, Phys. Lett. B **663**, 49 (2008).